Department of Precision and Microsystems Engineering

Data-based modal space control for active damping

Shiyu Fan

Report no : 2023.049
Coach : M.B. Kaczmarek
Professor : S.H. HosseinNia
Specialisation : Mechatronic System Design
Type of report : MSc Thesis
Date : 25 July 2023

DATA-BASED MODAL SPACE CONTROL FOR ACTIVE DAMPING

by

Shiyu FAN

to obtain the degree of Master of Science
at Delft University of Technology
to be defended publicly on Tuesday July 25, 2023 at 9:30.

by

Student number: 5444462
Project duration: September 1, 2022 – July 25, 2023
Thesis committee: S.H. HosseinNia, TU Delft,supervisor
M.B. Kaczmarek, TU Delft, daily supervisor
J.F.L. Goosen, TU Delft
M. Khosravi, TU Delft

CONTENTS

PREFACE

This chapter serves as a guide for the reader on how to efficiently go through the contents of this thesis.

Chapter 1 is the introduction chapter. The motivation for this thesis is presented by first explaining the need for active damping and introducing the idea of distributed sensing and actuation. Then, the need and the challenge of developing a new control architecture are presented.

Chapter 2 is the literature study for this project. Necessary background knowledge, such as the numeric model for the beam and piezoelectric material, the existing active damping methods, and the modal state estimation techniques, are discussed.

Chapter 3 is presented in a journal paper format, and it is self-contained. This is the main contribution of this thesis. First, section 3.1 to 3.3 provides the reader with a concise introduction to understand the problem and brief background knowledge to understand the proposed algorithm. Then, in section 3.4 the proposed method is explained. Finally, in section 3.5, the experimental setup for validating the algorithm and the final result is presented. Reading chapter 3 alone should be sufficient to understand the entirety of this thesis.

Chapter 4 serve as the further discussion of the proposed methods. All the relevant results from the experimental study and the simulation result are shown.

Chapter 5 conclude the main contribution of this thesis, and the potential improvements of this method are given.

For readers who are interested in further exploring this method and extending the experimental study, the Appendices section might be of interest: in Appendix A, the basic structure of the Labview program is shown. In Appendix B, the Matlab code that can be used to reproduce the result is given.

Shiyu Fan
Delft, July 2023

Abstract

This research presents a novel data-based modal control method for actively dampening the flexible mode in a multi-input multi-output (MIMO) system. Traditional passive damping methods add significant mass to the system, making recent advances in sensor and actuator technology, such as lightweight piezoelectric materials, a more appealing solution. The key contribution of this research is a novel modal decoupling method for active damping that uses the MIMO frequency response function to circumvent the need for a parametric model. This method facilitates the design of a single-input, single-output (SISO) controller that actively dampens a flexible mode using all available sensors and actuators. This approach significantly reduces the complexity of the controller design and tuning effort compared to the conventional decentralized control architecture. Experimental validation is carried out on a cantilever beam, which shows near-perfect isolation of the mode of interest. The study's findings may offer critical insights for future mechatronics systems, enabling the creation of more efficient and powerful machines.

ACKNOWLEDGEMENTS

First and foremost, I would like to thank Marcin, who not only allowed me the opportunity to explore this interesting topic but also generously shared his wisdom, guidance, and a wealth of practical knowledge. In addition, I also would thank Hassan as my main supervisor. The Monday morning gatherings were an enjoyable opportunity. It allows me to stay connected with fellow students and gain a concise understanding of their work. These exchanges played an important role in enhancing my knowledge in the field of Mechatronic System Design.

I feel deeply thankful for the chance to conduct my work in the Mechatronics lab in 3ME. Special thanks go to Francesco, Aditya, and all the dedicated individuals in the lab, for cultivating a supportive and enjoyable environment.

Finally, I extend my deepest gratitude to my family and friends for their ceaseless support; their encouragement was an indispensable factor in the completion of this journey.

Shiyu Fan
Delft, July 2023

1

INTRODUCTION

1

1.1. MOTIVATION

Moore's Law states that the number of transistors in integrated circuits will double approximately every two years. For the past 50 years, though its demise has become an enduring topic for many tech commentators, it has shown no signs of slowing down. This can be largely attributed to the advanced lithography processes enabling chip-makers to print even smaller features into the same area. Over the last decades, the improvement in the lithography system includes the introduction of immersion lithography, migration to shorter wavelengths,s and its recently advanced, increased numerical aperture (NA). However, adopting high NA for the optics system poses new challenges to the motion system [1]. This is because the new lens system will have the same resolution in X and Y directions. As a result, the fixed mask field size of 104mm × 132mm will image to a half field of 16.5mm × 26mm on the wafer instead of the conventional full field of 33mm × 26mm. As a result, faster stages are needed for the same productivity, specifically 4 times more acceleration for the mask stage and 2 times more for the wafer stage.

Facing such demanding requirements, the precision engineer can no longer rely on their traditional toolset, which only consists of masses and springs to produce predictable and repeatable behavior. To illustrate this, one example using the traditional design principle can be seen as a positioning system consisting of a monolithic leaf spring, as shown in figure 1.1.

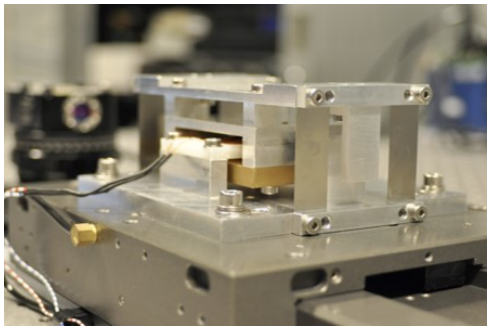

Figure 1.1.: Motion stage with parallel leaf spring

Such a structure can give the desired reproducible linear behavior and be free from hysteresis. However, design guided by the traditional approach usually neglects damping elements, so long-lasting vibration caused by resonance modes can be easily seen. This poses challenges for the control engineer, as vibration caused by resonance modes not only reduces the tracking performance but also limits the achievable bandwidth. One solution to this is to optimize the structure mass distribution such that the first resonance mode is at least five times above the required control bandwidth. Hence, the control system is not affected by the frequency of interest. However, as the demand for throughput and accuracy increases, such as in high-NA systems, the required control bandwidth will be pushed even higher, so the mechanical designer will be forced to achieve higher

natural frequencies. But it will soon become impossible to manufacture anymore.

When higher resonance frequency cannot be achieved by structure optimization, the control bandwidth will be severely limited. This is because, to reject disturbance, the performance of the feedback controller is limited by the dynamic behavior of the plant itself. The dynamics of the motion stage can be considered as a mass system where at low frequencies, it acts like a rigid body at high frequencies. However, multiple flexible modes will dominate the plant behaviors at resonance frequencies. As a result, these harmful vibration modes will limit the feedback control bandwidth because the phase will drop below -180° at the resonance frequency when the sensor and the actuator are not placed at the same degree of freedom. As illustrated by the previous example, elastic elements in the motion stage are typically designed to have low material damping to ensure precision and repeatability. However, a low damping value will manifest itself as the large encirclement in the Nyquist plot. This will, in turn, determines the maximum controller gain that will not lead to instability and, therefore, limits the accuracy of the motion stage when having disturbance. Traditionally, the flexible modes are taken care of by carefully placing notch filters at the resonances, but these filters will lower the phase and resulting low controller gain around the resonance when the disturbance is coming from outside. Thus, they will endanger the robustness of the feedback controller around the resonance.

In literature, many efforts have been devoted to increasing the damping of flexible modes in literature, either through passive damping or active damping.

1.2. DAMPING METHODS

Passive damping methods can be categorized into two groups, additional layer damping and tuned mass damper [2]. In the additional layer of damping, a viscoelastic material that will dissipate vibration energy is added to the original structure. In the tuned mass damper, one or multiple mass-spring systems are added to the original structure. The mass-spring system is calibrated to match one of the resonance frequencies of the original structure. As a result, the vibration energy of the original structure is transmitted to the tuned mass damper system. Thus, the amplitude of the vibration is reduced. Both of these methods are practical for industrial applications because they are free from adding energy sources and sensors/actuators. But their dissipative ability is proportional to the weight, so, in terms of high-tech application, the additional weight will not be favorable. Also, sensitivity to system variations such as temperature and loss of effectiveness for low-frequency mode make them unfavorable for high-tech applications.

Active damping methods also can be categorized as semi-active or fully active damping. Semi-active damping operates in the same way as passive damping, but it requires an additional power supply and controllable elements. One example of semi-active damping is shunt damping; it acts like a viscoelastic material but uses an electrical component to dissipate the vibration energy. It can dampen both low and high-frequency vibration via the tuning of electric elements, but the tuning process itself is complex and time-consuming because it requires the modification of the hardware itself and any change of component will influence the damping

performance. If the damping of a complex structure is required, the volume of the hardware itself may pose a challenge.

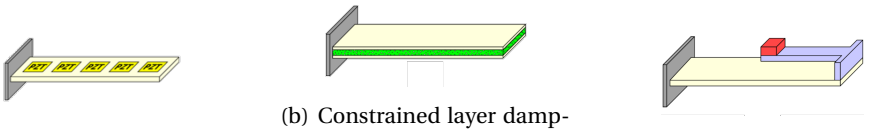

(a) Active damping (b) Constrained layer damping (c) Tuned mass damper

Figure 1.2.: Different damping methods [3]

The fully active damping consists of sensors, controllers, actuators, and an energy source. The vibration energy is dissipated by the counter-reaction force generated by the controller and actuator. The active damping methods not only have higher damping performance but also can provide low-mass and low-cost options compared to passive damping, which is suitable for high-tech applications. Additionally, by designing the control algorithm, requirements such as robustness against parameter variation and suppression against multiple modes can be achieved. So, active damping is a promising option for high-tech applications.

1.3. DISTRIBUTED SENSING AND ACTUATION

In many publications, examples of active vibration control for a beam or plate structure can be found using piezoelectric material acting as sensors and actuators in a distributed manner [4]. These advances in actuation and sensing with smart materials, such as piezoelectric material, allow more potential to improve the effectiveness of the control system, as the number of control surfaces and measurements can be increased with relatively low cost and difficulties. With the increased number of sensors and actuators, current challenges in vibration control such as the mass limitation in passive damping and the force limitation in active damping shall be overcome. A typical setup used for active vibration control of a flexible beam can be shown below:

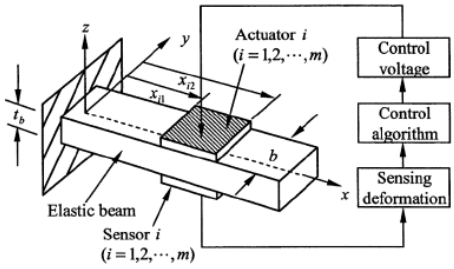

Figure 1.3.: Active vibration control with collocated transducer setup [5]

The strain of the beam can be sensed by piezoelectric sensors which are then passed through the controller, the output control voltage then will be applied to the piezoelectric actuators to generate a force that will oppose the unwanted deformation of the beam. In many examples, the piezoelectric element used as the sensor and actuator is attached to the same degree of freedom of the flexible structure. This is called the collocated configuration. This is advantageous for the distributed sensing and actuation because it is proved that this configuration can lead to phase behavior that will not exceed -180 degrees which guaranteed the stability of the system.

1.4. CHALLENGE FOR NEW CONTROL ARCHITECTURE

In literature, the control architecture of this collocated configuration can be categorized as decentralized control and centralized control.

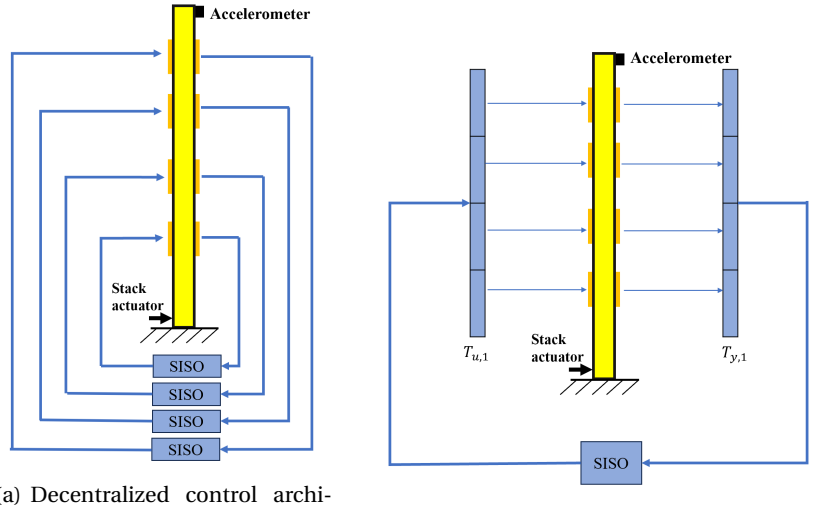

(a) Decentralized control architecture

(b) Centralized control architecture

Figure 1.4.: Decentralized and centralized control architecture

In figure 1.4a, the decentralized controller is achieved by restricting the actuator to only act on the data retrieved from the collocated sensor. Thus, the control problem can be divided into the design of multiple SISO control loops, each of which only has local information of the full structure. Though this type of control architecture has the advantages of reduced complexity and increased robustness against operational failure [6], it cannot guarantee optimal performance because no global information on the structure is used [7]. In figure 1.4b, the centralized control architecture will try to combine data from different sensors into one global quantity of the structure, and the control signal for different actuators is generated based on this global measurement, such as modal amplitude [8]. Because more information on the structure is used for the actuator, with a carefully designed controller, improved performance can be expected compared with the decentralized control architecture.

However, it still has a few drawbacks. First, more comprehensive information on the structure is needed to compute the global quantity. However, for a complex mechatronic system, a high-fidelity model based on the first principle, such as the finite element method, can be expensive and time-consuming to obtain. Second, the computation time will increase as the number of sensors and actuators increases, this limits its ability to meet the real-time control requirement [9].

In past studies, it has been experimentally demonstrated that the use of distributed sensing and actuation can improve damping performance in active vibration control with simplified control architecture [3]. The increased number of actuators and sensors, however, poses new challenges for the controller design, as the controller order and the number of tuning generally increased with the number of inputs and outputs. In many practical scenarios, low-order controllers with intuitive tuning rules are often more favorable, as the marginal improvement offered by high-order controllers might not compensate for the throughput lost due to the hassled tuning process. Therefore, the first challenge is to choose a controller architecture that can not only take the system's MIMO property into account but also offer a minimum number of tuning parameters for the designer.

The second challenge for the new control architecture comes from modeling. The model of a mechanical system is often derived using the first-principle-based method, such as Finite Element Methods(FEM) . However, in the high-tech industry, where the systems have become complex, the accuracy of such models becomes increasingly limited, as there will be a mismatch between the real physical geometry and the ideal assumption, as well as the material behavior. Thus, developing a full-order high-fidelity model with sufficient accuracy has come to an ever more resource-consuming task. To overcome these limits, the data-based approach has gained increasing attention. It is based on the assumption that, in practice, the frequency response function is accurate and cheap to obtain, so controller design directly based on the experimental input-output relationship can greatly reduce the dependency on the parametric model. However, there is a dilemma that exists as the parametric model provides an intuitive understanding of the underlying principle, but there is always a mismatch between real and theoretical models, the non-parametric model can provide an accurate description of the system with low cost, but it is not easy to interpret. Thus, a control architecture that not only can directly utilize the frequency response function but is also capable of giving physical insight is desired for the high-tech industry.

1.5. RESEARCH QUESTIONS

As illustrated in the previous chapter, the decentralized control architecture turns the design of the MIMO controller into the design of multiple SISO control loops, which only contain the diagonal element of the whole transfer function. To achieve better performance, attention has been given to centralized control architecture with minimum tuning parameters to better explore the MIMO property of the system. Also, to reduce the complexity of control architecture even further, the feedback control architecture should be as simple as possible so that it is possible to align

with the current design methodology in the high-tech industry, such as loop-shaping.

In the case of structural vibration control, global information such as modal amplitudes is desired to obtain as they can be computed from the sensors and used for distributed actuation. Again, while several state estimation techniques exist, such as the Luenberger observer and Kalman filter, favor is again given to techniques that only consist of a pair of the static matrix, such as modal filter and blended vectors as they offer simplicity and are well-suited for the mechanical system by explicit avoid the spillover effect.

Next, the computation modal information required knowing the mode shapes at different resonance frequencies. However, for complex mechatronic systems, high-fidelity parametric models needed for controller synthesis are not easy to obtain. Though many techniques for system identification can be found in literature, their performance still depends on the expertise of the engineer, and it is unclear how the poorly identified parametric models will influence the controller design. So, the synthesis of the controller directly based on the non-parametric model, such as the frequency response function obtained from the experiment, has become the standard practice in the high-tech industry. So, a novel controller design process that is compatible with nowadays standard industry practice will be explored.

Thus, the objective of this research is to develop a novel control architecture with distributed actuation and sensing suitable for vibration control that can answer the following question:

- How to develop a mode decoupling method for active damping in the distributed system that relies solely on the frequency response function?

From this research question, the following research objectives are defined:

- Develop an algorithm that can answer the research question.
- Design a distributed actuation and sensing setup and obtain the frequency response function for validation.
- Validate the proposed algorithm on the real frequency response function and test its performance in a real-time control loop.

REFERENCES

[1] Jan van Schoot. *AP3152 Optics for Lithography Session 12: High NA*. 2022.

[2] A. Preumont. "Vibration Control of Active Structures". In: Solid Mechanics and Its Applications 179 (2011). DOI: 10.1007/978-94-007-2033-6. URL: http://link.springer.com/10.1007/978-94-007-2033-6.

[3] T. van der Graaf. *Active Vibration Control: using over-sensing and over-actuation.* 2021.

[4] M. G. Schneiders, M. J. Van De Molengraft, and M. Steinbuch. "Benefits of over-actuation in motion systems". In: *Proceedings of the American Control Conference* 1 (2004), pp. 505–510. ISSN: 07431619. DOI: 10.23919/ACC.2004.1383653.

[5] Y. Yang, Z. Jin, and C. K. Soh. "Integrated optimal design of vibration control system for smart beams using genetic algorithms". In: *Journal of Sound and Vibration* 282.3-5 (Apr. 2005), pp. 1293–1307. ISSN: 0022-460X. DOI: 10.1016/J.JSV.2004.03.048.

[6] W. P. Engels, O. N. Baumann, S. J. Elliott, and R. Fraanje. "Centralized and decentralized control of structural vibration and sound radiation". In: (2006). DOI: 10.1121/1.2163270.

[7] S. J. Elliott. "Active control of structural vibration". In: *Solid Mechanics and its Applications* 130 (2005), pp. 1–19. ISSN: 18753507. DOI: 10.1007/1-4020-4161-6{_}1/COVER.

[8] A. Preumont, A. François, P. De Man, and V. Piefort. "Spatial filters in structural control". In: *Journal of Sound and Vibration* 265.1 (July 2003), pp. 61–79. ISSN: 0022-460X. DOI: 10.1016/S0022-460X(02)01440-2.

[9] G. Soto and H. Adeli. "Multi-agent replicator controller for sustainable vibration control of smart structures". In: *Journal of Vibroengineering* 19.6 (Sept. 2017), pp. 4300–4322. ISSN: 1392-8716. DOI: 10.21595/JVE.2017.18924. URL: https://www.extrica.com/article/18924.

2

LITERATURE REVIEW

2.1. PRELIMINARY

In this section, the model of the plant needs to be introduced. This is done by first applying Finite Element Method to a cantilever Euler-Bernoulli beam in section 2.1.1, as discussed in detail in [1]. Then the model of the piezoelectric element is derived in section 2.1.2 that is associated with the input and output of the plant. Finally, the modal decomposition technique is introduced 2.1.3 to approximate the continuum system with the lower order model.

2.1.1. BEAM MODELLING

Due to the small deformation of the beam, it can be modeled as the one-dimensional Euler-Bernoulli beam. It represents a linear elastic structure, and it can be combined with piezoelectric elements to determine the damping performance of a flexible system.

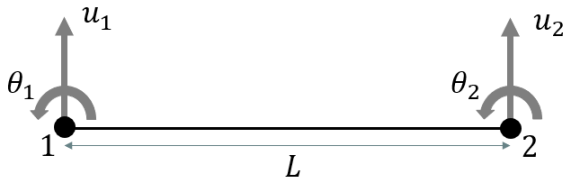

Figure 2.1.: Euler-Bernouilli FEM element

A beam element of length L consists of two nodes, and each node has a transnational degree of freedom u and rotational degree of freedom θ. Thus the nodal degree of freedom of the element $\bar{x_e}$ can be described as:

$$\bar{x_e} = \begin{bmatrix} u_1 \\ \theta_1 \\ u_2 \\ \theta_2 \end{bmatrix} \tag{2.1}$$

The property of each of the beam element is determined by its own four-by-four stiffness matrix K_e and mass matrix M_e, which is described as:

$$K_e = \frac{EI}{L^3} \begin{bmatrix} 12 & 6L & -12 & 6L \\ 6L & 4L^2 & -6L & 2L^2 \\ -12 & -6L & 12 & -6L \\ 6L & 2L^2 & -6L & 4L^2 \end{bmatrix} \tag{2.2}$$

$$M_e = \frac{\rho AL}{420} \begin{bmatrix} 156 & 22L & 54 & -13L \\ 22L & 4L^2 & 13L & -3L^2 \\ 54 & 13L & 156 & -22L \\ -13L & -3L^2 & -22L & 4L^2 \end{bmatrix} \tag{2.3}$$

Where E, I, ρ, A represent Young's modulus, density, the moment of inertia, and the cross-section area of the beam element, respectively.

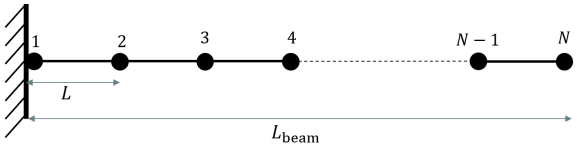

Figure 2.2.: Assembled beam model

Since the whole beam structure is modeled as multiple elements, the element matrix shown needs to be arranged by their corresponding nodal degree of freedom. After assembly, the equation of motion of the entire structure can be written as a second-order differential equation:

$$M\ddot{\bar{x}} + C\dot{\bar{x}} + K\bar{x} = B'\bar{f} \tag{2.4}$$

Where $M, K, \bar{f}$ are the system mass, stiffness matrix, input force, and B' determined which nodal degree of freedom the input force is acting on.C represent the system damping matrix. For simplicity, it can be modeled as the proportional damping: $C = \alpha M + \beta K$.

After deriving the equation of motion with a second-order differential equation, it is then converted to a set of first-order state space equations. This can be done by introducing a new state vector $\bar{d}$ with an additional state $\dot{\bar{x}}$ representing the velocity of the nodal degree of freedom.

$$\bar{d} = \begin{bmatrix} \bar{x} \\ \dot{\bar{x}} \end{bmatrix} \tag{2.5}$$

Then, the state space equation of the flexible system can be written as:

$$\begin{aligned} \dot{\bar{d}} &= \underbrace{\begin{bmatrix} 0 & I \\ -M^{-1}K & -M^{-1}C \end{bmatrix}}_{A_c} \bar{d} + \underbrace{\begin{bmatrix} 0 \\ -M^{-1}B' \end{bmatrix}}_{B_c} \underbrace{\bar{f}}_{\bar{u}} \\ &= A_c\bar{d} + B_c\bar{u} \end{aligned} \tag{2.6}$$

Where $A_c \in \mathbb{R}^{2n\times 2n}, B_c \in \mathbb{R}^{2n\times n_u}$ and $\bar{u} \in \mathbb{R}^{n_u\times 1}$, with n representing the number of nodes and n_u the amount of inputs.

The system output equation is shown in a similar way:

$$\bar{y} = C_c\bar{d} + D_c\bar{u} \tag{2.7}$$

Where $C_c \in \mathbb{R}^{n_y\times 2n}$ and $D_c \in \mathbb{R}^{n_y\times n_u}$ represent the output matrix and direct feed-through matrix, with n_y represents the amount of outputs.

From the above derivation, we can see that if the system's equation of motion is described in nodal space, then for complicated structures with n elements, we need a state space equation of $2n \times 2n$ to capture the dynamics of the system. However, in the field of high-tech industry, in order to achieve nano-meter accuracy, real-time control with a sampling rate at least 10 times higher than the dynamics range of

interest is required. In this situation, the high-fidelity model with a large degree of freedom posed a challenge for control implementation.

To solve this problem, a model reduction technique is needed to balance the ability to capture necessary dynamics and the computational limits. It will be discussed in detail in section 2.1.3.

2.1.2. PIEZOELECTRIC MODELLING

Piezoelectric materials are commonly used in active vibration control schemes. Because it has the benefit of fast response, high power density, and high signal-to-noise ratio. To examine how these materials could be included in the active vibration control framework, their working principle is first introduced.

Piezoelectric materials utilize the piezoelectric effect: when stress is applied, it will generate electric charges, which can be used to sense the deformation of the structure, and when the charge is applied, it will create mechanical deformation which can be controlled to counteract unwanted vibration.

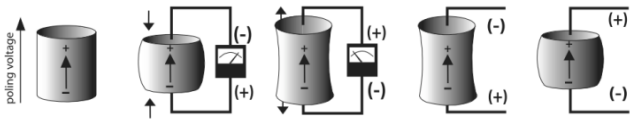

Figure 2.3.: Principle of piezoelectric element[2]

To describe these behaviors, the piezoelectric materials can be modeled as[3]:

$$\varepsilon_x = S_{11}^E \sigma_x + d_{31} E_z \tag{2.8}$$

$$D_z = d_{31} \sigma_x + \xi_{33}^\sigma E_z \tag{2.9}$$

where ε_x, S_{11}, d_{31}, E_z, D_z and ξ_{33} represent the strain, compliance, stress piezoelectric strain constant, electric field, electric displacement, and permittivity respectively. Equation 2.8 describes the actuation mode, and equation 2.9 describes the sensing mode of the piezoelectric material.

After the current is generated by electric charge, it can then be converted into a voltage signal that can be used in active control:

$$V^s(t) = Hze_{31} w \int_0^{l_p} n_2 \dot{u} dx = S\dot{u} \tag{2.10}$$

where H, z, e_31, w, l_p, and n_2 represent signal conditioning device gain, the distance to the neutral axis, piezoelectric stress constant, sensor width, sensor length, and the second spatial derivative of the shape function. After obtaining the voltage signal, the control voltage can be calculated and feedback to the actuator. The input voltage will cause the piezoelectric actuator to generate a bending moment that will attenuate unwanted vibration. The relationship between the applied voltage and the moment can be described as:

$$M_{act} = E_p d_{31} \bar{z} g V^s \tag{2.11}$$

where E_p, $\bar{z}$ and g represent Young's Modulus of the piezoelectric material, the distance to the neutral axis, and the control gain, respectively. Lastly, the relationship between the sensed structure deformation n_1 and the applied control force f_{act} can be described as:

$$f_{act} = E_p d_{31} w \bar{z} \left(g V^s\right) \int_0^{l_p} n_1^T dx \tag{2.12}$$

This relationship can be added as the input force to the Euler-Bernoulli beam model. And by replacing the corresponding mass and stiffness matrix of Euler-Bernoulli beam elements with Piezoelectric beam elements and adding to the system's total mass and stiffness matrix, the full parametric model can be set up to simulate the real system.

2.1.3. MODAL DECOMPOSITION

As mentioned in the previous section, the modal representation is useful because it allows for a low-order representation of high-order systems in a nodal form which often results from FE Modelling. It is based on the assumption that any physical vibration can be internally decoupled into a set of orthogonal vibration modes.

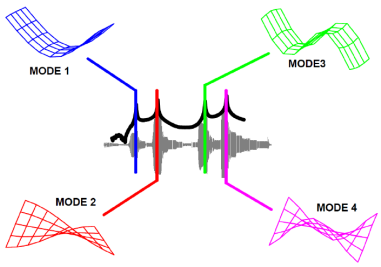

Figure 2.4.: Modal representation of the structure [4]

These orthogonal modes are obtained by solving the eigenvalue problem assuming the system is undriven ad undamped:

$$\left(K - \omega^2 M\right) \bar{v} = 0 \tag{2.13}$$

where ω and $\bar{v}$ represent the natural frequency and vibration modes. Then, the vibration of the system can be seen as the superposition of N vibration modes:

$$\begin{aligned} \bar{x} &= \eta_1 \bar{v}_1 + \eta_2 \bar{v}_2 + \eta_3 \bar{v}_3 + \ldots \eta_N \bar{v}_N \\ &= \underbrace{\begin{bmatrix} \bar{v}_1 & \bar{v}_2 & \bar{v}_3 & \ldots & \bar{v}_N \end{bmatrix}}_{\Phi} \underbrace{\begin{bmatrix} \eta_1 \\ \eta_2 \\ \eta_3 \\ \vdots \\ \eta_N \end{bmatrix}}_{\bar{z}} \\ &= \Phi \bar{z}, \end{aligned} \tag{2.14}$$

where η_i represent the modal participation factor of vibration mode $\bar{v}_i$. Thus, the transformation matrix Φ can be obtained by collecting N vibration mode $\bar{v}_i$ which represents the transformation from physical coordinates $\bar{x}$ to a set of orthogonal coordinates $\bar{z}$.

The constant transformation matrix Φ is also called the mode shape matrix. With this transformation $\bar{x} = \Phi\bar{z}$ and left multiply the nodal equation of motion by Φ, the modal form is obtained:

$$\Phi^T M\Phi\ddot{\bar{z}} + \Phi^T C\Phi\dot{\bar{z}} + \Phi^T K\Phi\bar{z} = \Phi^T B'\bar{f} \tag{2.15}$$

By the scaling of Φ, we can define $\Phi^T M\Phi = I$ and $\Phi^T K\Phi = \Omega^2$ where Ω^2 containing of the natural frequency $\Omega^2 = \text{diag}\begin{bmatrix} \omega_1^2 & \omega_2^2 & \dots & \omega_N^2 \end{bmatrix}$. Thus, a simpler modal equation of motion can be obtained:

$$\ddot{\bar{z}} + \Phi^T C\Phi\dot{\bar{z}} + \Omega^2\bar{z} = \Phi^T B'\bar{f} \tag{2.16}$$

Again, these second-order differential equations can be rearranged to the state-space form by defining a new state vector $\bar{q} = \begin{bmatrix} \bar{z} \\ \dot{\bar{z}} \end{bmatrix}$:

$$\dot{\bar{q}} = \underbrace{\begin{bmatrix} 0 & I \\ -\Omega^2 & -\Phi^T C\Phi \end{bmatrix}}_{A_{cm}}\bar{q} + \underbrace{\begin{bmatrix} 0 \\ \Phi^T B' \end{bmatrix}}_{B_{cm}}\underbrace{\bar{f}}_{\bar{u}} \tag{2.17}$$

It is worth noting that if proportional damping is assumed, then the damping matrix C can be diagnosed by Φ, as $\Phi^T C\Phi = 2Z\Phi$ where $Z = \text{diag}(\zeta_1, \dots, \zeta_n)$ which contains the modal damping ratio ζ_i of each mode. By applying the same procedure to the measurement matrix, the complete state space equation in modal form can be obtained:

$$\begin{aligned} \dot{\bar{q}} &= A_{cm}\bar{q} + B_{cm}\bar{u} \\ \bar{y} &= C_{cm}\bar{q} + D_{cm}\bar{u} \end{aligned} \tag{2.18}$$

2.2. ACTIVE DAMPING METHOD

This chapter will provide an overview of some general Active Vibration Control methods. It will show the most generally adopted method in literature, but it is far from complete. The methods that will be presented include classical Single-Input-Single-Output controllers like the Integral resonance control in section 2.2.1, Direct velocity feedback in section 2.2.2, Positive position feedback in section 2.2.3. The idea of presenting these classical methods is to partly answer the first research question in section 1.5 as the design of these classical controllers can rely on the frequency response, rather than the parametric model as introduced in 1.4 . Also, this chapter will also include methods that can deal with Multi-Input-Multiple-Output systems, such as the Full state feedback in section 2.2.4 and Independent modal space control present in section 2.2.5.

2.2.1. INTEGRAL RESONANCE CONTROL

An algorithm commonly seen in literature when piezoelectric materials are used is the Integral resonance control(IRC) [5]. The principle of the Integral Resonance Control can be explained in Figure

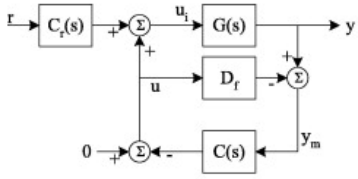

(a) Controller in IRC configuration

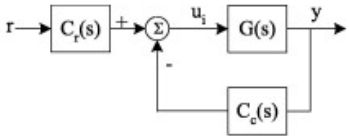

(b) Controller in conventional feedback configuration

Figure 2.5.: Integral resonant control [5]

The transfer function $G(s)$ represents a structure with weakly damped modes:

$$G(s) = \sum_{i=1}^{M} \frac{A_i}{s^2 + 2\zeta_i \omega_i s + \omega_i^2} \tag{2.19}$$

The tuning objective of the Integral Resonance Controller is to determine the feed-through term D_f and the controller $C(s)$ such that the damping ratio of the targeted mode is increased. The design of the feed-through term D_f is to add zero at a frequency lower than the lowest resonant frequency. For the design of D_f, the reader is referred to [5] for more detail. Several choices of the controller $C(s)$ have been suggested, for example, the controller can be an integral control:

$$C(s) = -\frac{K}{s} \tag{2.20}$$

The gain of the term K can be found using the conventional frequency domain tool, such as root locus [6]. Though damping can be added to the system via an integrator. However, the integrator will introduce phase lag behavior thus will limit the bandwidth of the system. Also, it will lead to high control input at low frequency which might lead to actuator saturation. The application of this method can be found in [7] where it is used to active damped the flexible mode in the robot manipulator and in [8] it is used to increase the performance of a piezoelectric nanopositioning stage.

2.2.2. DIRECT VELOCITY FEEDBACK

If the governing equation of the structure is assumed as [9]:

$$M\ddot{x} + Kx = bu \tag{2.21}$$

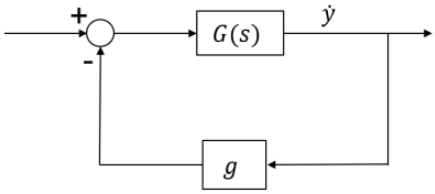

Figure 2.6.: Principle of Direct Velocity Feedback

It is straightforward to see the damping of the structure can be increased by modifying the velocity term. The control algorithm that employs this idea is called Direct Velocity Feedback(DVF).

It uses the output signals from velocity sensors:

$$y = b^T \dot{x} \tag{2.22}$$

The control signal is obtained by multiplying output by a control gain g:

$$u = -g\,y \tag{2.23}$$

Thus the closed-loop equation can be written as:

$$M\ddot{x} + gbb^T \dot{x} + Kx = 0 \tag{2.24}$$

In the literature, the DVF has been found to be unconditionally stable for a collocated system. But there are several disadvantages. At high frequencies, due to the constant feedback gain, DVF does not have sufficient roll-off, and it tends to utilize high control force at all frequencies. Also, it may become closed-loop unstable when the actuator dynamics are considered [10]. Finally, if displacement sensors are used instead of velocity sensors, it will require an additional differentiator, which will increase high-frequency noise [11].

2.2.3. POSITIVE POSITION FEEDBACK

DVF is not suitable for every kind of system, and for example, some systems do not exhibit the roll-off of $-40dB/decade$, which is caused by a feed-through compliance term due to the model truncation. Thus, Positive Position Feedback(PPF) is introduced by Goh and Caughey [12] to solve this problem. It uses the position output of the system and multiple it by a second-order filter:

$$H(s) = \frac{-g}{s^2 + 2\xi_f \omega_f s + \omega_f^2} \tag{2.25}$$

where the g, ξ_f and ω_f are the tuning parameters of the filter.

The stability condition of the closed loop can be found as [13]:

$$gG(0)C(0) < 1 \tag{2.26}$$

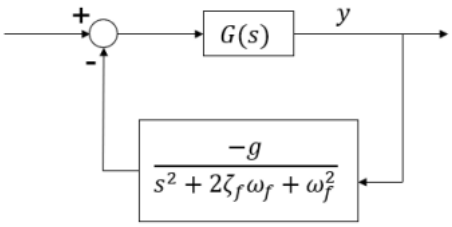

Figure 2.7.: Principle of Positive Position Feedback [9]

Due to the low-pass nature of the second-order filter, it can deal with noise and dynamics at high frequencies. However, the PPF can only dampen the targeted mode when the ω_f of the filter is closed to the natural frequency of the targeted mode ω_i[14]. Thus it requires knowledge of the natural frequency of the structure, when the natural frequency structure is time-varying, an adaptive algorithm may be needed to modify the ω_f of the filter.

Different variations of Positive Position Feedback can be found in the literature. In order to deal with frequency variation in the structure, the frequency estimator is combined with Positive Position Feedback in [15] and [16], which is able to suppress multiple time-variant resonances in the structure. A fractional order version of Positive position feedback is proposed in [11], which demonstrates it can mitigate the spillover effect from the uncontrolled modes. In [17], a modified version of Positive Position Feedback is proposed, in which a first-order compensator is added to the second-order controller, it has shown significant improvement in steady-state response in the experiment.

2.2.4. FULL STATE FEEDBACK

Many active vibration controllers in literature can only be used for Single-Input-Single-Output systems, but many complex mechatronics systems now require Multi-Input-Multi-Output controllers because only considering the diagonal term of the transfer function is not sufficient to meet the requirement. In this section, attention is paid to a method [18] that uses the estimated modal states to add stiffness and damping in order to deal with the flexible dynamics of the system. By introducing additional stiffness and damping into the system, the phase behavior that hinders the achievement of higher bandwidth in the feedback controller is improved [19]. And we would particularly focus on how the full-state feedback is used to add damping to the system.

First, the second-order equation for one degree of freedom system is introduced [20]:

$$\ddot{\eta} = -\omega^2\eta - 2\zeta\omega\dot{\eta} + \phi_a^\top u \tag{2.27}$$

where ω and ζ represent the natural frequency and modal damping, η represent the modal state and $\phi_a^\top$ denotes the influence of input u to this mode. After the state

$\hat{x} = \begin{bmatrix} \hat{\eta} & \dot{\hat{\eta}} \end{bmatrix}^\top$ have been obtained by the observer[21], the feedback input u_{sf} is obtained by introducing feedback gain $K = \begin{bmatrix} K_s & K_d \end{bmatrix}$:

$$\begin{aligned} u_{sf} &= \begin{bmatrix} K_s & K_d \end{bmatrix} \begin{bmatrix} \hat{\eta} \\ \dot{\hat{\eta}} \end{bmatrix} \\ &= \begin{bmatrix} K_s & K_d \end{bmatrix} \left(\begin{bmatrix} \eta \\ \dot{\eta} \end{bmatrix} - \begin{bmatrix} e_\eta \\ \dot{e}_\eta \end{bmatrix} \right) \end{aligned} \tag{2.28}$$

where $e_\eta = \eta - \hat{\eta}$ represent the estimation error. By including the u_{sf} in the input u, we could find how to modify the stiffness and damping of the one degree of freedom system by K_s and K_d:

$$\begin{aligned} \ddot{\eta} &= -\omega^2 \eta - 2\zeta\omega\eta + \phi_a^\top \left(u + u_{sf} \right) \\ &= \left(-\omega^2 + \phi_a^\top K_s \right) \eta + \left(-2\zeta\omega + \phi_a^\top K_d \right) \dot{\eta} + \phi_a^\top u + \phi_a^\top \left(K_s e_\eta + K_d \dot{e}_\eta \right) \end{aligned} \tag{2.29}$$

We can examine the effect of the state feedback term K_d in Figure We could observe from the pole-zero map that by only changing the real part of the corresponding pole, we can modify the peak of the resonance without changing the natural frequency and the zero is not affected by the additional control force because it only depends on the sensor and actuator configuration.

After showing the term K_d can indeed change the damping property of the system, three different ways of tuning the K_d term are proposed: *a*) Automatic manual tuning, *b*) Minimizing the interaction between modes and *c*) Pole placement. The detail of these methods will not be explained here, but the reader can refer to [20] if needed.

2.2.5. INDEPENDENT MODAL SPACE CONTROL

In order to deal with the spillover effect of the full state feedback controller which may cause instability, a control method that is able to each mode separately was proposed in [22], which is called Independent Modal Space Control. It uses the orthogonality principle of the mode shapes to design the controller. It requires knowing the modal state of the targeted mode, so it can be classified as the centralized controller. To obtain this modal state, different state estimation algorithms can be used, such as the Modal filter, Luenberger observer, and Kalman filter. After the modal states have been calculated, any kind of Single-Input-Single-Output controller can be added to the control loop because the system has been decoupled into orthogonal vibration modes.

Many variations of this technique can be found in the literature. The Modified Independent Modal Space Control proposed in [23], [24] aims at using a limited amount of actuators to control many modes. It achieves this by choosing to only dampen the vibration mode that has the largest vibration energy in a time instance. In [25], this MIMSC method is combined with Positive Position Feedback which shows better transient behavior. Attempts are also made by combining the Independent Modal Space control with other controllers such as PID [26],[27], and LQR controller [28].

2.3. MODAL STATE ESTIMATION

The general problem of state estimation can be formulated as how to estimate the modal state $\bar{x}_{k+1}$ from an incomplete measurement $\bar{y}_k$ when using the state space description of the system introduced. In the case of estimating the modal states of mechanical structures, the measurable states $\bar{y}_k$ could be the strain value at specific locations of the beam. All the classical estimation methods mentioned in this chapter require obtaining the state-space model of the system. It can be achieved either through building a first-principle model or identifying the state-space model using system identification techniques.

LUENBERGER OBSERVER

The topic of state estimation has been studied for decades in the field of systems and control. One of the most widely adopted techniques is the Luenberger observer [29].

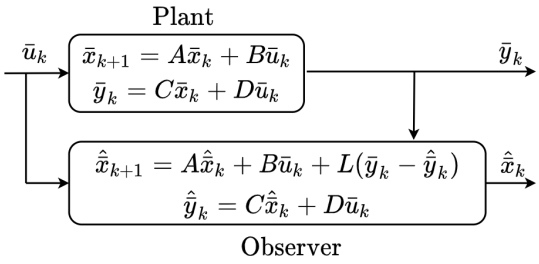

Figure 2.8.: State observer framework [30]

First, a discrete linear time-invariant model without noise is assumed.

$$\begin{aligned} \bar{x}_{k+1} &= A\bar{x}_k + B\bar{u}_k \\ \bar{y}_k &= C\bar{x}_k + D\bar{u}_k \end{aligned} \tag{2.30}$$

where at the instance k, $\bar{x}_k$ represents the the modal states of the structure, $\bar{u}_k$ is its input and $\bar{y}_k$ is the measurable outputs. Suppose the correct structure model can be obtained, then in the observer design. In that case, an additional term can be included in the model such that using the successive values of the input $\bar{x}_k$ and output $\bar{y}_k$ of the plant, the estimated modal state $\hat{\bar{x}}_k$ will converge to the real modal state $\bar{x}_k$. More specifically, a matrix L can be introduced to ensure the converging of the estimated modal states by multiplying the measurement error $(\bar{y}_k - \hat{\bar{y}}_k)$ by L. The dynamics of the observer can thus be formulated as:

$$\begin{aligned} \hat{\bar{x}}_{k+1} &= A\hat{\bar{x}}_k + B\bar{u}_k + L\left(\bar{y}_k - \hat{\bar{y}}_k\right) \\ \hat{\bar{y}}_k &= C\hat{\bar{x}}_k + D\bar{u}_k \end{aligned} \tag{2.31}$$

Defining the error of the observer as $\tilde{\bar{x}}_k = \bar{x}_k - \hat{\bar{x}}_k$, it dynamics thus can be found as:

$$\tilde{\bar{x}}_{k+1} = (A - LC)\tilde{\bar{x}}_k \tag{2.32}$$

Since the system matrix A and C are fixed, their dynamics it fully governed by choice of observer gain L. For the discrete system, the Luenberger observer is therefore stable if all of the eigenvalues of matrix $A-LC$ are inside the unit circle. Because a large observer gains L can be chosen as long as it is stable, in an ideal situation, the error of the states $\tilde{\bar{x}}_k$, therefore, can converge to zero arbitrarily fast. However, in the most practical situation, a large observer gain L will amplify high-frequency noise $\bar{v}_k$ thus compromising the accuracy of the estimated modal state $\hat{\bar{x}}_k$. Also, in the case where the process noise $\bar{w}_k$, which may represent the model uncertainty, can not be ignored, this type of observer design will result in an inaccurate estimation of the modal state $\hat{\bar{x}}_k$. These two influences can then be formulated as follows:

$$\tilde{\bar{x}}_{k+1} = (A-LC)\tilde{\bar{x}}_k + L\bar{v}_k + \bar{w}_k \tag{2.33}$$

In case when the Luenberger observer is used to estimate the state of mechanical structure, another drawback is worth drawing attention to. Because the dynamics of the structure are usually derived in modal form, after which the modal truncation is applied to only preserve the modes within a finite frequency range. So, a distinction is made between the modeled modes and unmodelled modes. The problems thus arise are defined as spillover effects [31]. More specifically, the observation spillover is the effect of the energy of unmodelled modes influencing the measurements $\hat{\bar{y}}_k$, and the control spillover is the control energy of unmodelled modes influence the true modal states $\bar{x}_{k+1}$. It has been shown in the literature that the combined effects of observer spillover and control spillover can lead to instability. Thus, unless a careful selection of the observer gain L is performed, the spillover effect will limit the use of the Luenberger observer in active vibration control.

KALMAN FILTER

As discussed earlier, traditional observers like Luenberger observers assumed a deterministic system because no measurement noise or process noise is taken into account. This often limits its full use in real mechatronic systems as it may lead to performance degradation. In this section, another classical state estimation algorithm is introduced. Namely, the Kalman filter [32].

The Kalman filter has numerous applications ranging from guidance and navigation of vehicles to robotic motion planning and even econometrics. It is based on the assumption that errors have a Gaussian distribution because the primary sources of excitation to a dynamics system can be thought of as independent Gaussian random processes with zero mean. To take the process and measurement noise into account, the state space equation of the original system can be written as [33]:

$$\begin{aligned} \bar{x}_{k+1} &= A\bar{x}_k + B\bar{u}_k + \bar{w}_k \\ \bar{y}_k &= C\bar{x}_k + D\bar{u}_k + \bar{v}_k \end{aligned} \tag{2.34}$$

where $\bar{w}_k$ and $\bar{v}_k$ represent process and measurement noise. Each of them is assumed to be a Gaussian distribution with zero means: $w_k \sim \mathcal{N}(0,Q)$ and $v_k \sim \mathcal{N}(0,R)$. Here Q and R represent the covariance matrix of process and measurement noise respectively.

The Kalman filtering works by a two-step process, namely the prediction step and the update step. In the prediction process, a prediction about current state $\hat{\bar{x}}_{k|k-1}$ is calculated based on the estimated state $\hat{\bar{x}}_{k-1|k-1}$ and input $\bar{u}_{k-1}$ at the previous time step using the state space model.

Next in the prediction step, the covariance matrix of the next state $P_{k|k-1}$is also updated, as the $P_{k|k-1}$ is defined as $E\left[\left(\bar{x}_k - \hat{\bar{x}}_{k|k-1}\right)\left(\bar{x}_k - \hat{\bar{x}}_{k|k-1}\right)^T\right]$:

$$P_{k|k-1} = AP_{k-1|k-1}A^T + Q \tag{2.35}$$

In the update step, the new measurement at the current time $\bar{y}_k$ is obtained and is used to correct the prediction in the previous step. First, unbiased and minimum variance estimation of the current state $\hat{\bar{x}}_{k|k}$ is calculated using measurement signal $\bar{y}_k$ and Kalman gain K:

$$\begin{aligned} \hat{\bar{x}}_{k|k} &= \hat{\bar{x}}_{k|k-1} + K_k\left(y_k - C\hat{\bar{x}}_{k|k-1}\right) \\ K_k &= P_{k|k-1}C^T\left(CP_{k|k-1}C^T + R\right)^{-1} \end{aligned} \tag{2.36}$$

Then, the covariance matrix is also updated:

$$P_{k|k} = P_{k|k-1} - K_kCP_{k|k-1} \tag{2.37}$$

In literature, one of the main advantages of the Kalman filter is it will make an LQ-optimal trade-off between the prediction step and the update step based on the assumed covariance matrix Q and R. It will result in an unbiased and minimum variance estimation of the state [30].

However, there still are several drawbacks of the Kalman filter worth mentioning. First, though it is proven to be an optimum estimation algorithm based on certain assumptions, it does yield the existence of an intuitive tuning rule for the parameters Q and R. It is often said that the Q matrix implies confidence in the model, as large Q will cause the filter to put more weight on the measurement signal, and the R matrix implies confidence in the measurement, as large R will lead to the filter to rely more on the model rather than measurement output. As the uncertainty in the model or in measurement can not be directly quantified in the covariance matrix, tuning the matrix itself can be tedious and will greatly influence the filter's performance. Second, the estimation algorithm introduced so far, including the Luenberger observer and Kalman filter, all require knowing the input to the system. However, this may not be available to all mechatronic systems as input force may result from unwanted disturbance caused by the feed-forward signal. Though this problem may be solved by developing new kinds of estimation algorithms [30], the new method will often add more computational complexity. Lastly, though the Kalman filter can compensate for the model uncertainty using measurement, it still requires the state space model derived from the first principle. In the high-tech industry, design methodology directly based on obtained input-output relationship has gained increasing attention in recent years, as the accuracy of the model instead of advanced model-based control technique is the main obstacle for achieving higher throughput in precision motion systems.

MODAL FILTER

For mechanical systems, as this is the case for most high-tech equipment, another well-known modal state estimation technique can be used, namely the modal filter.

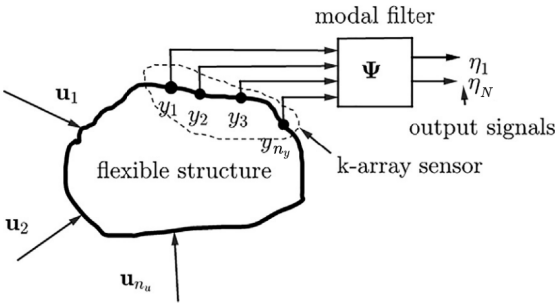

Figure 2.9.: Representation of modal filter [34]

It was first proposed to solve the spillover problem using an observer, and it is based on the principle of the orthogonality of the mode shapes of the mechanical system [35]. In the most used case, an array of sensors and actuators are placed on the surface of the structure, output of the sensors is weighted using a static matrix to produce a virtual signal only sensitive to a specific mode. The virtual signal is then passed through a single-input-single-output controller, and the actuators' control signal is distributed so that they can only actuate one mode. There are many methods that can derive the modal filter, but the derivation using Finite Element Model will be illustrated in this section.

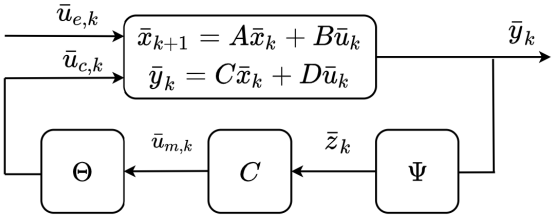

Figure 2.10.: General modal control scheme[30]

The process of the design of the modal filter using the FE Model can be derived as follow: the obtained sensor outputs $\bar{y} = \begin{bmatrix} y_1 & \dots & y_{n_s} \end{bmatrix}^T$ are multiply by a static matrix Ψ which will linear transform the outputs to modal contribution $\bar{z} = \begin{bmatrix} \eta_1 & \dots & \eta_N \end{bmatrix}^T$.In the classical modal filter design, the modal description of the underlying mechanical system is needed. This has been done in the previous chapter as follows:

$$\ddot{\bar{z}} + \Phi^T C \Phi \dot{\bar{z}} + \Omega^2 \bar{z} = \Phi^T B' \bar{u} \tag{2.38}$$

Then, the measurement equation also needs to be defined:

$$\bar{y} = C_z \Phi \bar{z} + C_{\dot{z}} \Phi \dot{\bar{z}} + D\bar{u} \tag{2.39}$$

where Φ represents the transformation from nodal to modal coordinate and C_z and $C_{\dot{z}}$ represent the location of the position and velocity sensors, respectively. It can be rewritten in matrix form as [36]:

$$\bar{y} = \begin{bmatrix} \bar{y}_p \\ \bar{y}_v \end{bmatrix} = \underbrace{\begin{bmatrix} C_z\Phi & 0 \\ 0 & C_{\dot{z}}\Phi \end{bmatrix}}_{H} \begin{bmatrix} \bar{z} \\ \dot{\bar{z}} \end{bmatrix} \tag{2.40}$$

Since we already obtained the relationship between the measurement signal $\bar{y}$ and modal quantity $\dot{z}, \dot{\bar{z}}$. The static matrix Ψ can therefore be calculated as the inverse of H: $\Psi = H^{-1}$, such that:

$$\begin{bmatrix} \bar{z} \\ \dot{\bar{z}} \end{bmatrix} = \Psi \begin{bmatrix} \bar{p} \\ \bar{v} \end{bmatrix} \tag{2.41}$$

However, in a situation where matrix H is not a square matrix, other techniques to find the general inverse, such as the Moore–Penrose inverse can be used[37]. The modal filer Ψ can therefore be calculated as:

$$\Psi = \left(H^T H\right)^{-1} H^T \tag{2.42}$$

After the modal quantity such as $\dot{z}, \dot{\bar{z}}$ are obtained, the SISO modal controller can be designed to change the dynamics of the specific mode. Lastly, the control forces generated by individual controllers can also be obtained in a similar manner. The relationship between the modal force $\bar{u}_m$ and the nodal force can be denoted by matrix R:

$$\bar{u}_m = \underbrace{\Phi^T B}_{R} \bar{u} \tag{2.43}$$

Then, the nodal force is derived using the pseudoinverse:

$$\bar{u} = \underbrace{\left(R^T R\right)^{-1} R^T}_{\Theta} \bar{u}_m \tag{2.44}$$

It is worth noting that since the SISO controller is already constrained in the modal space, the modal controller can be any type of controller, such as PID. It is not limited to Positive Position Feedback if only a selected number of modes need to be damped.

Besides being constructed from the orthogonality condition of mode shapes, the modal filter can also be obtained directly from experimental data, as in [38]. The author proposed a method that shows how to obtain the weighting factor α_i for each sensor after the individual frequency response function has been obtained. It mainly relies on the use of pseudo-inverse to calculate the weighting factor α_i such that, within a given bandwidth $[\omega_a, \omega_b]$, the measured frequency response can be summed to the mass-spring-damper system with unit amplitude at resonance.

In this section, various methods that can estimate the modal state is introduced, such as the Luenberger Observer, Kalman Filter, and Modal filter. However, since an accurate parametric model is assumed to be challenging to obtain in the project, then other methods do not need the parametric model needs to be investigated. Therefore, in this section, the Experimental modal analysis techniques are introduced in 2.3.

EXPERIMENTAL MODAL ANALYSIS

As mentioned in the previous section, the parametric model obtained from the Finite Element Method is not suitable for designing controllers for the complex mechatronic system. The reason can be attributed to various modeling errors, such as geometric and material properties mismatch, the boundary conditions do not correspond to the idealized assumption, such as the rigid supports, and it can also be caused by inexperienced users, such as choosing poor element sizes or shapes, specifying the wrong element types or getting the incorrect data input.

In order to obtain the modal information from the real structure, a technique called Experimental Modal Analysis is well-studied in the literature. Within the broad field of Experimental Modal Analysis, we can generally categorize different methods into two types: Experiment Modal Analysis(EMA) and Operational Modal Analysis(OMA). The Experiment Modal Analysis represents traditional modal testing as the structure is excited by one or several measured dynamics forces. It is considered a well-established technique in mechanical engineering that has many applications in the aerospace, automotive, and heavy equipment industries. But it is not suitable for situations where it is difficult to excite or measure the excitation or reproduce the exact boundary condition of the structure. Therefore, Operational Modal Analysis is developed [39] which is suitable for the structure that is operating conditions rather than laboratory conditions. It has the most applications in civil engineering because the structure's response is often due to ambient excitation or operational loading, such as wind or traffic. Therefore the input signal is not available. Though the Operational Modal Analysis has the advantage of being an output-only algorithm, it still has several drawbacks worth mentioning, such as it is only capable of producing non-physical modes due to input force and noise and the absolute scaling of mode shapes is not possible because it requires to measure the driving point.

In [41], various methods related to the Experimental Modal Analysis are investigated. In general, the procedure for modal analysis can be summarized in three steps: first, the frequency range of interest is selected to keep the order of the model at an acceptable level. Second, complex conjugate pole pairs are identified from frequency response data. Third, the mode shape vectors are identified based on the selected poles. After obtaining the modal model from the data, various applications can be found in the literature [42],[43], such as structural health monitoring and model updating.

In [44], the experimental side of this method is introduced. As shown in Figure 2.12, various measurement tools, the accelerometer in this case, are attached to the structure. The shaker on the right will excite the structure at the specified

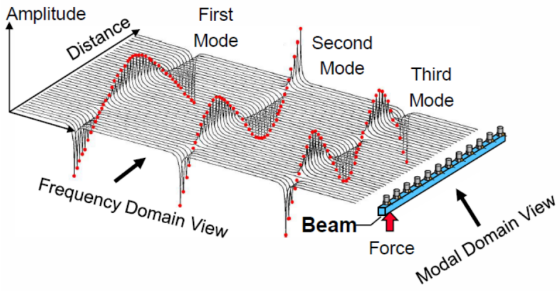

Figure 2.11.: Relationship between frequency domain and modal domain[40]

frequency band, and a column of frequency response function will be recorded for each excitation location. Many excitation signals have been developed to facilitate frequency domain analysis [45]. After the experiment, modal information such as natural frequency, damping ratio, and mode shape can be extracted from data using various algorithms.

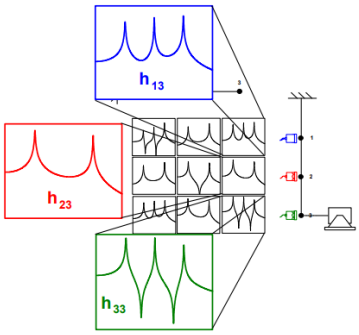

Figure 2.12.: Illustration of shaker test [44]

After obtaining the data from the experiment, Modal parameter estimation techniques can be used to identify the relevant modal parameters. Two types of methods, namely the Peak Picking and Frequency domain decomposition method, will be shortly introduced here. Peak Picking is mostly used in civil engineering due to its simplicity and intuitiveness. It estimates the resonance frequency from the peaks in frequency response function [46], the damping value from the bandwidth, and the mode shapes are estimated from the peaks of frequency response at the resonance. However, this method might fail when the assumptions of well-separated eigenfrequencies and low damping are violated, and it obtains the operational deflection shapes at the resonance rather than the mode shapes. Though these two concepts are closely connected, see [47], just obtaining the operational deflection shapes in the spatial domain does not necessarily guarantee the orthogonality of different "mode shapes". Therefore, a more rigorous method which is the

Frequency domain decomposition is used [48]. Its working principle can be seen as decomposing the spectral matrix into a set single-degree-of-freedom system using the Singular Value Decomposition and then identifying the single-degree-of-freedom model from the singular value curve and, lastly, identifying the modal parameters from the single-degree-of-freedom model. In order to identify the modal parameter from the singular value curve in figure 2.13, curve fitting methods need to be used. In [45], all curve fitting techniques can be summarized into four groups: *a*) local single degree of freedom, *b*) local multiple degrees of freedom, *c*) global, and *d*) multi-reference. The reader is referred to [45] for more details.

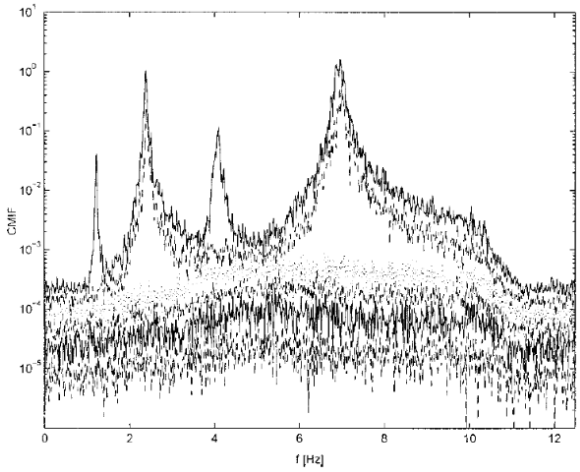

Figure 2.13.: SVD curve of a flexible system [49]

REFERENCES

[1] R. D. Cook, D. S. Malkus, M. E. Plesha, and R. J. W. Witt. “Concept and Applications of Finite Element Analysis”. In: (2002), p. 733.

[2] S. O. Reza Moheimani. “Piezoelectric Transducers for Vibration Control and Damping”. In: *Piezoelectric Transducers for Vibration Control and Damping* (2006). DOI: 10.1007/1-84628-332-9.

[3] K. G. Aktas and I. Esen. “State-Space Modeling and Active Vibration Control of Smart Flexible Cantilever Beam with the Use of Finite Element Method”. In: *Engineering, Technology & Applied Science Research* 10.6 (2020), pp. 6549–6556. ISSN: 1792-8036.

[4] P. Avitabile. “Experimental Modal Analysis-A Simple Non-Mathematical Presentation EXPERIMENTAL MODAL ANALYSIS (A Simple Non-Mathematical Presentation)”. In: (2001).

[5] A. Al-Mamun, E. Keikha, C. S. Bhatia, and T. H. Lee. “Integral resonant control for suppression of resonance in piezoelectric micro-actuator used in precision servomechanism”. In: *Mechatronics* 23.1 (Feb. 2013), pp. 1–9. ISSN: 0957-4158. DOI: 10.1016/J.MECHATRONICS.2012.10.001.

[6] S. S. Aphale, A. J. Fleming, and S. O. Reza Moheimani. “Integral resonant control of collocated smart structures”. In: *Smart Materials and Structures* 16.2 (Feb. 2007), p. 439. ISSN: 0964-1726. DOI: 10.1088/0964-1726/16/2/023.

[7] E. Pereira, S. S. Aphale, V. Feliu, and S. O. Moheimani. “Integral resonant control for vibration damping and precise tip-positioning of a single-link flexible manipulator”. In: *IEEE/ASME Transactions on Mechatronics* 16.2 (Apr. 2011), pp. 232–240. ISSN: 10834435. DOI: 10.1109/TMECH.2009.2039713.

[8] M. Namavar, A. J. Fleming, M. Aleyaasin, K. Nakkeeran, and S. S. Aphale. “An analytical approach to integral resonant control of second-order systems”. In: *IEEE/ASME Transactions on Mechatronics* 19.2 (2014), pp. 651–659. ISSN: 10834435. DOI: 10.1109/TMECH.2013.2253115.

[9] A. Preumont. “Vibration Control of Active Structures”. In: Solid Mechanics and Its Applications 179 (2011). DOI: 10.1007/978-94-007-2033-6. URL: http://link.springer.com/10.1007/978-94-007-2033-6.

[10] M. J. Balas. “Direct Velocity Feedback Control of Large Space Structures”. In: *https://doi-org.tudelft.idm.oclc.org/10.2514/3.55869* 2.3 (May 2012), pp. 252–253. ISSN: 07315090. DOI: 10.2514/3.55869.

[11] L. Marinangeli, F. Alijani, and S. H. HosseinNia. “Fractional-order positive position feedback compensator for active vibration control of a smart composite plate”. In: *Journal of Sound and Vibration* 412 (Jan. 2018), pp. 1–16. ISSN: 0022-460X. DOI: 10.1016/J.JSV.2017.09.009.

[12] C. J. Goh. “Analysis and Control of Quasi Distributed Parameter Systems”. In: (1983). DOI: 10.7907/96PH-6521.

[13] J. L. Fanson. “An Experimental Investigation of Vibration Suppression in Large Space Structures Using Positive Position Feedback”. In: (1987). DOI: 10.7907/0SA8-HW86.

[14] G. Song, S. P. Schmidt, and B. N. Agrawal. “A Complex Analytic Solution for the Attitude Motion of a Near-Symmetric Rigid Body Under Body-Fixed Torques”. In: *Celestial Mechanics and Dynamical Astronomy* 25.1 (1967), pp. 69–75. DOI: 10.2514/2.4865. URL: http://arc.aiaa.org.

[15] H. Hani Ihab Mohammad AlHasni. *Adaptive Multimodal Damping of Flexible Structures*. 2021.

[16] K. H. Rew, J. H. Han, and I. Lee. “Multi-Modal Vibration Control Using Adaptive Positive Position Feedback”. In: *Journal of Intelligent Material Systems and Structures* 13.1 (July 2016), pp. 13–22. ISSN: 1045389X. DOI: 10.1177/1045389X02013001866.

[17] S. Nima Mahmoodi and M. Ahmadian. “Active vibration control with modified positive position feedback”. In: *Journal of Dynamic Systems, Measurement and Control, Transactions of the ASME* 131.4 (July 2009), pp. 1–8. ISSN: 00220434. DOI: 10.1115/1.3089565/466077.

[18] K. W. Verkerk, Y. Kasemsinsup, H. Butler, and S. Weiland. “State estimator synthesis for position dependent flexible systems with position independent error convergence”. In: *2015 23rd Mediterranean Conference on Control and Automation, MED 2015 - Conference Proceedings* (July 2015), pp. 1065–1070. DOI: 10.1109/MED.2015.7158898.

[19] K. W. Verkerk, H. Butler, and P. P. Van Den Bosch. “Improved disturbance rejection for high precision systems through estimation of the flexible modes”. In: *2015 IEEE Conference on Control and Applications, CCA 2015 - Proceedings* (Nov. 2015), pp. 1191–1196. DOI: 10.1109/CCA.2015.7320774.

[20] K. K. Verkerk. “Improved accuracy of flexible systems by state estimation : applied to high-precision motion systems”. In: (2018).

[21] K. W. Verkerk, J. Achterberg, C. M. Van Lierop, and S. Weiland. “Modal observer design for a flexible motion system with state dependent sensor positions”. In: *Proceedings of the IEEE Conference on Decision and Control* (2012), pp. 4498–4504. ISSN: 25762370. DOI: 10.1109/CDC.2012.6426444.

[22] L. Meirovitch and H. Baruh. “CONTROL OF SELF-ADJOINT DISTRIBUTED-PARAMETER SYSTEMS.” In: *AIAA Paper* (1980), pp. 1–10. ISSN: 01463705. DOI: 10.2514/6.1980-1707.

[23] A. Baz and S. Poh. “Performance of an active control system with piezoelectric actuators”. In: *Journal of Sound and Vibration* 126.2 (Oct. 1988), pp. 327–343. ISSN: 0022-460X. DOI: 10.1016/0022-460X(88)90245-3.

[24] A. Baz, S. Poh, and P. Studer. “Modified Independent Modal Space Control Method for Active Control of Flexible Systems”. In: *Proceedings of the Institution of Mechanical Engineers, Part C: Mechanical Engineering Science* 203.2 (Mar. 1989), pp. 103–112. ISSN: 0263-7154.

[25] A. Baz, S. Poh, and J. Fedor. “Independent Modal Space Control With Positive Position Feedback”. In: *Journal of Dynamic Systems, Measurement, and Control* 114.1 (Mar. 1992), pp. 96–103. ISSN: 0022-0434. DOI: 10.1115/1.2896512.

[26] S. Etedali. “A new modified independent modal space control approach toward control of seismic-excited structures”. In: *Bulletin of Earthquake Engineering* 15.10 (Oct. 2017), pp. 4215–4243. ISSN: 15731456. DOI: 10.1007/S10518-017-0134-6/FIGURES/12.

[27] S. Etedali, M. R. Sohrabi, and S. Tavakoli. “An Independent Robust Modal PID Control Approach for Seismic Control of Buildings”. In: *Journal of Civil Engineering and Urbanism* 3.5 (2013), pp. 279–291.

[28] R. E. Lindberg and R. W. Longman. “On the Number and Placement of Actuators for Independent Modal Space Control”. In: *https://doi-org.tudelft.idm.oclc.org/10.2514/3.56366* 7.2 (May 2012), pp. 215–221. ISSN: 07315090. DOI: 10.2514/3.56366. URL: https://arc-aiaa-org.tudelft.idm.oclc.org/doi/10.2514/3.56366.

[29] D. G. Luenberger. “An Introduction to Observers”. In: *IEEE Transactions on Automatic Control* 16.6 (1971), pp. 596–602. ISSN: 15582523. DOI: 10.1109/TAC.1971.1099826.

[30] P. de Bruin. *Input and state estimation for compliant motion stages: Estimating modal contribution for guidance flexures*. 2022.

[31] L. Meirovitch and H. Baruh. “On the problem of observation spillover in self-adjoint distributed-parameter systems”. In: *Journal of Optimization Theory and Applications* 39.2 (Feb. 1983), pp. 269–291. ISSN: 00223239. DOI: 10.1007/BF00934533/METRICS.

[32] R. E. Kalman. “A New Approach to Linear Filtering and Prediction Problems”. In: *Journal of Basic Engineering* 82.1 (Mar. 1960), pp. 35–45. ISSN: 0021-9223. DOI: 10.1115/1.3662552.

[33] M. Verhaegen and V. Verdult. “Filtering and system identification: A least squares approach”. In: *Filtering and System Identification A Least Squares Approach* 9780521875127 (Jan. 2007), pp. 1–405. DOI: 10.1017/CBO9780511618888.

[34] A. Preumont, A. François, P. De Man, and V. Piefort. “Spatial filters in structural control”. In: *Journal of Sound and Vibration* 265.1 (July 2003), pp. 61–79. ISSN: 0022-460X. DOI: 10.1016/S0022-460X(02)01440-2.

[35] L. Meirovitch and H. Baruh. “The implementation of modal filters for control of structures”. In: *https://doi-org.tudelft.idm.oclc.org/10.2514/3.20045* 8.6 (May 1984), pp. 707–716. ISSN: 07315090. DOI: 10.2514/3.20045.

[36] M. I. Friswell. “ON THE DESIGN OF MODAL ACTUATORS AND SENSORS”. In: *Journal of Sound and Vibration* 241.3 (Mar. 2001), pp. 361–372. ISSN: 0022-460X. DOI: 10.1006/JSVI.2000.3300.

[37] W. Gawronski. “Modal Actuators and Sensors”. In: *Advanced Structural Dynamics and Active Control of Structures* (June 2004), pp. 203–218. DOI: 10.1007/978-0-387-72133-0{_}8.

[38] A. Preumont, A. François, P. De Man, and V. Piefort. “Spatial filters in structural control”. In: *Journal of Sound and Vibration* 265.1 (July 2003), pp. 61–79. ISSN: 0022-460X. DOI: 10.1016/S0022-460X(02)01440-2.

[39] F. B. Zahid, Z. C. Ong, and S. Y. Khoo. “A review of operational modal analysis techniques for in-service modal identification”. In: *Journal of the Brazilian Society of Mechanical Sciences and Engineering* 42.8 (Aug. 2020), pp. 1–18. ISSN: 18063691. DOI: 10.1007/S40430-020-02470-8/FIGURES/2.

[40] Brüel & Kjær. *Operational Modal Analysis OMA*. 2013. URL: https://www.bksv.com/en/knowledge/training/training-courses/denmark/university/live-courses/operational-modal-analysis/oct-5-2023.

[41] M. Böswald, D. Göge, U. Füllekrug, and Y. Govers. “A Review of Experimental Modal Analysis Methods with respect to their Applicability to Test Data of Large Aircraft Structures”. In: (2006).

[42] P. Thankachan, A. Raj, R. Kumar Garg, and A. Raj $. “Structural Health Monitoring using Experimental Modal Analysis Structural Health Monitoring by Modal Analysis View project Structural Health Monitoring Using Experimental Modal Analysis”. In: (2016).

[43] A. Zanarini. “Full field optical measurements in experimental modal analysis and model updating”. In: *Journal of Sound and Vibration* 442 (Mar. 2019), pp. 817–842. ISSN: 0022-460X. DOI: 10.1016/J.JSV.2018.09.048.

[44] P. Avitabile. “Experimental modal analysis : A simple non-mathematical presentation”. In: *Sound and Vibration* (Sept. 2017), pp. 1–35. DOI: 10.1002/9781119222989.CH1.

[45] B. J. Schwarz and M. H. Richardson. “EXPERIMENTAL MODAL ANALYSIS”. In: (1999).

[46] H. Naderpour and P. Fakharian. “A Synthesis of Peak Picking Method and Wavelet Packet Transform for Structural Modal Identification”. In: *KSCE Journal of Civil Engineering* 20.7 (2016), pp. 2859–2867. ISSN: 1976-3808. DOI: 10.1007/s12205-016-0523-4.

[47] M. H. Richardson. “Is It a Mode Shape, or an Operating Deflection Shape”. In: (1997).

[48] R. Brincker, L. Zhang, and P. Andersen. “Modal identification of output-only systems”. In: *Smart Materials and Structures* 10.3 (June 2001), p. 441. ISSN: 0964-1726. DOI: 10.1088/0964-1726/10/3/303.

[49] B. Peeters and G. D. Roeck. “Stochastic System Identification for Operational Modal Analysis: A Review”. In: *Journal of Dynamic Systems, Measurement, and Control* 123.4 (2001), pp. 659–667. ISSN: 0022-0434.

3

DATA-BASED MODAL SPACE CONTROL FOR ACTIVE DAMPING

ABSTRACT *This paper presents a novel data-based modal control method for actively dampening the flexible mode in a multi-input multi-output (MIMO) system. Traditional passive damping methods add significant mass to the system, making recent advances in sensor and actuator technology, such as lightweight piezoelectric materials, a more appealing solution. The key contribution of this paper is a novel modal decoupling method for active damping that uses MIMO frequency response function to circumvent the need for a parametric model. This method facilitates the design of a single-input, single-output (SISO) controller that actively dampens a flexible mode using all available sensors and actuators. This approach significantly reduces the complexity of the controller design and tuning effort compared to the conventional decentralized control architecture. Experimental validation is carried out on a cantilever beam, which shows near-perfect isolation of the mode of interest. The study's findings may offer critical insights for future mechatronics systems, enabling the creation of more efficient and powerful machines.*

3.1. INTRODUCTION

To meet the growing demand for more advanced products, the efficiency and accuracy of the machinery involved in their production must constantly improve. This principle applies across all sectors where precision and throughput are the key factors, especially the semiconductor industry. However, the flexible modes in the machine will cause unwanted vibration and limit the maximum achievable bandwidth of the controller [1]. Therefore, it is desired to dampen these flexible modes. Conventional passive damping methods, such as tuned mass damper and constrained layer damping, have been proven effective [2], but they will add too much mass to the system. Recent advances in sensor and actuator technology, such as lightweight piezoelectric material, give new possibilities to incorporate control systems to actively dampen these flexible modes.

In the active vibration control (AVC) community, these piezoelectric materials are usually placed in collocated pairs to act as actuators and sensors. Sometimes, an array of collocated pairs are needed to provide sufficient damping performance. However, as the number of actuators and sensors increases, it will usually complicate the controller design, as it is not intuitive to see how each actuator input and sensor output is related to the damping performance of a specific mode. This problem can be generally considered a Multi-input multi-output (MIMO) problem, and specifically controlling a mode in the system is known as Independent Modal Space Control (IMSC) [3], and achieving it often requires knowing the modal coordinates of the vibration modes. For the mechanical system, this modal coordinate can be obtained using a state estimator or a modal filter [4]. However, constructing such a state estimator or a modal filter generally requires us to obtain an accurate parametric model of the system in advance. But it is often time-consuming for the industry to obtain a parametric model with enough accuracy, especially for a complex mechatronic system having many flexible modes and with many actuators and sensors.

Alternatively, we can use the information from the frequency response function (FRF) as the non-parametric model to design the modal control scheme. Because the FRD model can describe the Linear-Time Invariant (LTI) system accurately, we can obtain it from the experiment at a low cost. Several methods in literature have discussed how to decouple the system to avoid the excitation of the flexible modes. For example, Watchi in [5] uses the Singular Value Decomposition to decouple the six rigid body modes from the flexible modes. Vaes [6] proposed an optimization scheme to obtain the decoupling matrix, which guarantees robust performance. Qian [7] tries to use the closed-loop subspace identification method to identify the modal state-space model to achieve mode decoupling between modal coordinates. And Stoev in [8] calculates the transformation matrix for decoupling by tensor decomposition. Though all of those methods demonstrate the ability to decouple the mode in the system, none of them attempt to incorporate the property of the system into the algorithm to simplify the problem. On the one hand, by not considering the system's physical property, we have gained an advantage in terms of wider applicability when using the algorithm for different kinds of systems. On the other hand, we tend to lose efficiency by not best utilizing the physical property of

the system, especially when only the mechanical system is of concern.

Therefore, the main purpose of this paper is to develop an alternative modal decoupling method aimed at applying active damping. This method will only use the MIMO frequency response function instead of the parametric model. Also, in contrast to the state-of-the-art data-based method, we will try to incorporate the property of the mechanical system into the algorithm to have a numerically efficient method. This might lead to the loss of versatility for the proposed method, but it will provide an efficient alternative for mode decoupling when only the mechanical system is of concern. As a result, this method will allow us to use one Single-input, single-output (SISO) controller to actively dampen a flexible mode independently while using all of the sensors and actuators available.

3.2. LOCAL ACTIVE DAMPING

In this section, we will first introduce the ideal of distributed actuation and sensing and why it is more advantageous in terms of controlling flexible mode in section 3.2.1. In section 3.2.2, we will discuss why it is more beneficial to implement the centralized control architecture than the decentralized control architecture. Lastly, in section 3.2.3, we will present the practical challenge of implementing centralized control and how this research will tackle this challenge.

3.2.1. DISTRIBUTED ACTUATION AND SENSING

Active control of the unwanted flexible modes is envisaged as an important challenge for the future mechatronics system [9], as these pronounced flexible modes will appear in the frequency range around the control bandwidth [10]. In traditional motion control design, the plant is assumed to be only dominated by the rigid-body mode, the excitation of unwanted flexible modes is avoided by placing the actuators or sensors at the nodes of the flexible modes. Therefore, there is insufficient controllability and observability of the flexible modes in the motion control loop. However, for the AVC loop, the goal is to actively dampen these modes, so an alternative approach that intends to maximize the controllability and observability of these modes should be pursued to provide sufficient damping performance.

Unlike the rigid-body modes in the six Degrees of Freedom (DOF), the flexible modes will cause complex spatial deformations of the structure. These deformations manifest as interactions between sensor outputs and actuator inputs, which can be interpreted as complex directionality within the MIMO system. To deal with the multi-variable nature of the flexible modes, the concept of distributed actuation and sensing is employed, where a number of small actuators and sensors are spatially distributed on the flexible structures [11]. This distributed actuation and sensing configuration is in sharp contrast with the conventional motion control loop, where only a minimum number of actuators and sensors for the six DOFs is preferred, but it can ensure that the sensors can provide better observability of the modes and the damping force of the actuators will be better aligned with the complex mode shapes.

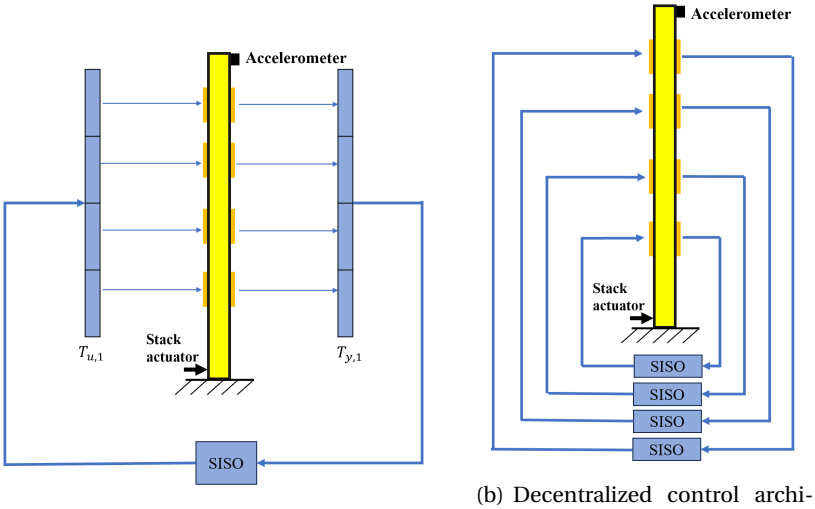

(a) Centralized control architecture

(b) Decentralized control architecture

Figure 3.1.: Centralized control and decentralized control architecture

3.2.2. LOCAL ACTIVE DAMPING METHODS

For the aforementioned distributed actuation and sensing configuration, there are generally two different control strategies: namely, the centralized and decentralized control [12], as shown in Figure 3.1. In centralized control, as shown in figure 3.1a, the outputs from all the sensors are combined as a centralized control signal, and this centralized control signal will pass through the controller and then be redistributed to different actuators. When the structure's vibration is of concern, this centralized control signal will often correspond to certain vibration amplitudes or mode shapes. In decentralized control, on the other hand, the output of the sensors will not be combined but directly sent to the respective controller, and then the controller's output will go to the corresponding actuator.

In the AVC setup, the actuator and sensor pair for the decentralized control will often be placed in a collocated configuration, which means they will be located at the same degree of freedom, as shown in figure 3.1b. This is because, in the collocated configuration, the controller can only provide a finite amount of energy. Therefore, the stability of the controller is robust against the parasitic modes [13]. But if they are in the non-collocated configuration, the controller may cause instability because of the parasitic flexible dynamics [14]. The collocated configuration is also favorable regarding the practical implementation, as the design step can be summarized as measuring the response between collocated pair and then designing the controller for this open-loop frequency response.

Different AVC controllers can be implemented based on different sensor types [12]. When the velocity sensor is available, the sensor output can be direct feedback to the actuator with static gain, which is called Direct Velocity Feedback (DVF). When

the force sensor is used, the Integral Resonance Control (IRC) can be implemented with a displacement actuator. When the collocated piezoelectric patch is considered, Positive Position Feedback (PPF) is preferred because the piezoelectric sensor will act as a position sensor. This position response is positive feedback, which allows the actuator to apply a force with an opposite phase with respect to the displacement.

3.2.3. MOTIVATION FOR DATA-BASED MODAL DAMPING

The damping performance of the decentralized architecture has been experimentally verified in [12],[11], where multiple collocated piezoelectric patches are used to dampen the flexible mode. In literature, the vibration in the structure is often described as the superposition of vibration mode, which consists of the mode shapes, eigenfrequencies, and modal coordinates [15]. However, the decentralized control architecture is only in terms of local variables, for example, the local strain distribution, rather than the modal coordinates. Therefore, the order of the control system will increase with the increased inputs and outputs. For practical implementation, the lower-order controller is usually preferred for the ease of tuning. Therefore, an alternative approach is to transform the local coordinates into global modal coordinates and subsequently design a SISO controller for a specific modal coordinate. In this way, the number of controllers we need to design will be the same as the targeted modes instead of depending on the number of inputs and outputs.

However, the practical difficulties of transforming the local coordinates into global modal coordinates lie in obtaining an accurate parametric model that can describe the MIMO system's behavior. In the case of achieving active vibration control using piezoelectric materials, this parametric model needs to capture the mechanical, piezoelectric, and electronic properties of the system accurately [13]. In literature, the parametric model that corresponds to the exact physical system can either be derived using Finite Element Modeling (FEM) software or by fitting a lower order transfer function on the obtained experimental data, but using both of these approaches will face the trade-off between the accuracy of the model and the time and resources it worth spending [16].

Alternatively, the physical system can also be described using a non-parametric model, such as the frequency response function, which can be obtained with high accuracy and low cost [16]. In section 3.1, we have briefly discussed some of these methods from the literature, but none of these methods explicitly address the problem of decoupling the flexible mode for active damping purposes. Also, the principle behind them is not straightforward to understand. Therefore, in section 3.3 and 3.4 we will propose a new data-based method that aims at decoupling the flexible mode from the system for active damping. The working principle behind this method will mostly be based on the mechanical insight of the system, so it would be easier for an engineer with a mechanical background to understand. Lastly, the performance of this method will be validated on a flexible cantilever in section 3.5.

3.3. BACKGROUND

3.3.1. PROBLEM FORMULATION

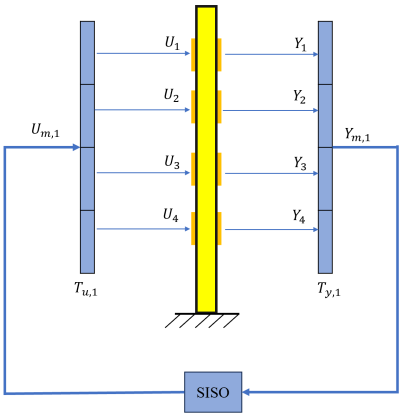

Figure 3.2.: In this figure, a cantilever beam with collocated piezoelectric patches are used as the distributed actuation and sensing system. From the right side, all the sensor signals Y_i will be combined by vector $T_{y,1}$ to become a scalar value $Y_{m,1}$, which will correspond to the modal amplitude of a flexible mode. After the SISO controller, the modal input signal $U_{m,1}$ will be distributed by vector $T_{u,1}$ to become the separate actuator signals U_i. This will ensure the controller can only excite the mode to be controlled.

In this section, we will first introduce the necessary mathematical expression in order to formulate the problem:

- $G(s) \in \mathbb{C}^{n_y \times n_u}$ represents the transfer function for a second-order mechanical system with n_u actuators and n_y sensors.
- $U \in \mathbb{R}^{n_u \times 1}$ represents the actuator signals for n_u actuators.
- $Y \in \mathbb{R}^{n_y \times 1}$ represents the sensor signals for n_y sensors.
- $U_{m,i} \in \mathbb{R}$ represents the modal actuator signal for the i^{th} mode.
- $Y_{m,i} \in \mathbb{R}$ represents the modal sensor signal for the i^{th} mode.

The idea of modal control, as introduced in Section 3.2.3, is to find a set of static coordinated transformations with unit length $T_{y,i} \in \mathbb{R}^{n_y \times 1}$ and $T_{u,i} \in \mathbb{R}^{n_u \times 1}$ for the i^{th} mode, such that all the sensor signals Y are combined into a modal sensor signal $Y_{m,i} \in \mathbb{R}$ as:

$$Y_{m,i} = T_{y,i}^T Y, \tag{3.1}$$

and all the actuator signals U are distributed to generate a modal control signal $U_{m,i} \in \mathbb{R}$ as:

$$U = T_{u,i} U_{m,i}. \tag{3.2}$$

In this way, the dynamics of other modes are isolated from the i^{th} mode to be controlled. With the modal control signal $U_{m,i}$ and the modal sensor signal $Y_{m,i}$, a SISO modal controller $SISO_i(s)$ can then be designed for the targeted i^{th} vibration mode using n_y sensors and n_u actuators. Finally, the closed-loop block diagram for the modal control scheme is shown in Figure 3.3, and a more graphic way of representing the close loop is shown in 3.2.

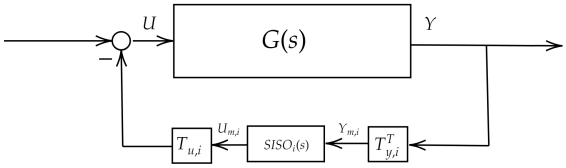

Figure 3.3.: The block diagram for close-loop interconnection

3.3.2. MATHEMATICAL PRELIMINARY

To develop the modal control scheme as described in Section 3.3.1, we first need to quantify what is the modal controllability and observability of $T_{u,i}$ and $T_{y,i}$ for a given system $G(s)$. Therefore, in Definition 1, $\mathcal{H}_2$ norm is chosen to be the measurement for the modal controllability and observability. In literature, other ways to quantify the modal controllability and observability, such as the $\mathcal{H}_\infty$ norm and the Hankel norm, have been introduced [17]. But using $\mathcal{H}_2$ norm as the measurement together with the Definition 2 and the Lemma 1, will provide a computationally efficient way to compute the modal filter $T_{u,i}$ and $T_{y,i}$.

Definition 1 *Quantify the efficiency of modal controllability and observability [18]: Assume the transfer function $G(s)$ represents a second-order flexible mode with n_u inputs and n_y outputs, the $T_{u,i} \in \mathbb{R}^{n_u \times 1}$ and $T_{y,i} \in \mathbb{R}^{n_y \times 1}$ are the modal transformation vectors with unit length. Then, the efficiency factor η is defined to quantify the modal controllability and observability of $T_{u,i}$ and $T_{y,i}$:*

$$\eta = \frac{\left\| T_{y,1}^T G(s) T_{u,1} \right\|_{\mathcal{H}_2}}{\|G(s)\|_{\mathcal{H}_2}}, \tag{3.3}$$

where $\|G(s)\|_{\mathcal{H}_2}$ represents the $\mathcal{H}_2$ norm of $G(s)$.

Here, the goal is to find the vectors $T_{u,i}$ and $T_{y,i}$ such that the efficient factor η is maximized. In Equation 3.3, because the changes in $T_{u,i}$ and $T_{y,i}$ will not change the value of the denominator, which is the $\mathcal{H}_2$ norm of $G(s)$, the denominator then can be taken out of the optimization process. Therefore, Equation 3.3 can also be rewritten as:

$$\eta = \left\| T_{y,1}^T G(s) T_{u,1} \right\|_{\mathcal{H}_2} \tag{3.4}$$

To solve the problem in Definition 1, the $\mathscr{H}_2$ norm of the system needs to be evaluated in each optimization step. For the mechanical system, however, the evaluation of the $\mathscr{H}_2$ norm can be simplified using the following Lemma:

Lemma 1 *$\mathscr{H}_2$ norm of second-order system [19]:*
Assume the SISO transfer function $g(s)$ represents an asymptotically stable and strictly proper second-order system, its $\mathscr{H}_2$ norm can be found as:

$$\|G\|_{\mathscr{H}_2} = \sqrt{\zeta\omega_n}\left|g(j\omega_n)\right| \tag{3.5}$$

where η and ω_n represent the damping ratio and natural frequency of the system $g(j\omega)$.

Therefore, evaluating the $\mathscr{H}_2$ norm can be turned into evaluating the modulus of a complex number.

Lastly, Definition 2 proposed a numerically efficient way to find the modulus of the complex number.

Definition 2 *Obtain the modulus of a complex number z [20]:*
The modules of a complex number z can be found by maximizing the function $f(\theta)$ over variable θ:

$$|z| = \max_{\theta\in\mathbb{R}} f(\theta), \tag{3.6}$$

where $f(\theta)$ is defined as:

$$f(\theta) = \Re(z)\cos\theta + \Im(z)\sin\theta. \tag{3.7}$$

3.4. DATA-BASED MODAL ACTIVE DAMPING — THEORY

In this section, we will introduce how to construct the modal filter $T_{y,i}$ and $T_{u,i}$ introduced in Section 3.3 from the frequency response function.

First, we will introduce the definition of input and output mode shape: the input mode shape vector $T'_{u,i} \in \mathbb{R}^{n_u\times 1}$ represents how each actuator will excite the i^{th} mode, and the output mode shape vector $T'_{y,i} \in \mathbb{R}^{1\times n_y}$ represents how each sensor will sense the deformation of the i^{th} mode. These definitions will show how the directionality of each mode shape is reflected in the input-output relationship of the MIMO system, and it will allow us to circumvent the process of obtaining a full modal model of the plant.

In step 1 of section 3.4, we will use the input mode shape $T'_{u,i}$ as an illustration to explain how to obtain the input/output mode shape from the frequency response function. Then to facilitate the mode decoupling, we will divide the mode shape that we obtained in step 1 into two categories: the specific mode we want to control and the rest of the modes that we want to isolate. Then, in step 1 of section 3.4, the null space of the modes we want to isolate is also calculated, which will be used in the subsequent step.

Then, in step 2 of section 3.4, we will show how to calculate the modal filter $T_{y,i}$ and $T_{u,i}$ from the frequency response function. It is often the case that

fusion of inputs and outputs, as shown in figure 3.2, will result in a drop in the controllability and observability of the system [18]. So, in this step, we will show how to calculate the vector $T_{y,i}$ and $T_{u,i}$ so that they have the optimum controllability and observability over the mode to be controlled. This optimality is quantified in terms of the H_2 norm as in Definition 1. Also, we will best utilize the property of the mechanical system to simplify the problem introduced in equation 3.19 of step 2. The result will be a numerically efficient algorithm that allows us to directly obtain $T_{y,i}$ and $T_{u,i}$ from the frequency response function, which will have maximum controllability and observability over the mode to be controlled.

As the final step, after we calculate the vectors $T_{y,i}$ and $T_{u,i}$ using the proposed approach, a SISO controller can be implemented as shown in figure 3.2.

Step 1: Mode decoupling:

Assuming there are a total of n_m modes that we want to isolate from the mode we want to control. We can collect all the input and output mode shape vectors $T'_{u,i}$ and $T'_{y,i}$ from the n_m^{th} modes we want to isolate and concatenate them in the matrix T'_u and T'_y as:

$$T'_u = \begin{bmatrix} T'^T_{u,1}; & \cdots & ; T'^T_{u,n_m} \end{bmatrix},$$

and

$$T'_y = \begin{bmatrix} T'_{y,1}; & \cdots & ; T'_{y,n_m} \end{bmatrix}.$$

To prevent the dynamics of other modes from entering the targeted mode, their null space is computed respectively as:

$$N_u = \mathcal{N}(T'_u) \tag{3.8}$$

and

$$N_y = \mathcal{N}(T'_y), \tag{3.9}$$

where the $\mathcal{N}(T'_u)$ denotes finding the null space of matrix T'_u.

These null spaces N_u and N_y will be used in the subsequent step to compute the modal transformation vectors $T_{u,i}$ and $T_{y,i}$. It is worth noting that if the T'_u and T'_y are matrices with full rank, then we can not have the solution for the null space where the dynamics of other modes can be isolated. This also implies that for a limited number of actuators and sensors, the total number of modes we are able to isolate is finite.

To compute the aforementioned null space N_u and N_y from the frequency response function, we first need to obtain all the input mode shapes vectors $T'_{u,1} \dots T'_{u,n_m}$ and output mode shapes $T'_{y,1} \dots T'_{y,n_m}$. To compute the vector $T'_{u,i}$, for example, we first parameterize it in an n_u dimensional sphere coordinates with $n_u - 1$ angular coordinates $\varphi = [\varphi_1, \varphi_2, \dots, \varphi_{n_u-1}]$, where all the angles ranging from $[-\pi, \pi)$ [21]. The reason for this parametrization is that we only want to know the direction of the input mode shape $T'_{u,i}$ instead of its magnitude, so using sphere coordinates would be sufficient. Also by using the sphere coordinates, we could reduce the total number of variables to $n_u - 1$ instead of n_u, which reduces the

computational time for the subsequent optimization problem. Therefore, the vector $T'_{u,i}$ can be rewritten as:

$$T'_{u,i} = \begin{bmatrix} \sin(\varphi_1)\dots\sin(\varphi_{n_u-2})\sin(\varphi_{n_u-1}) \\ \sin(\varphi_1)\dots\sin(\varphi_{n_u-2})\cos(\varphi_{n_u-1}) \\ \vdots \\ \sin(\varphi_1)\cos(\varphi_2) \\ \cos(\varphi_1) \end{bmatrix}. \tag{3.10}$$

Second, to recover the optimum direction in which the input mode shape $T'_{u,i}$ represented in this system's input and output relationship [22], we would examine the frequency response of $M(\omega_i)$, which is defined at the natural frequency of the first mode ω_i:

$$M(\omega_i) = G(\omega_i)\mathcal{N}(T_{u,i}). \tag{3.11}$$

If the $\mathcal{N}(T_{u,i})$ shows no excitation in $M(\omega_i)$, we can recover the optimum direction of $T'_{u,i}$. This can be formulated as an optimization problem where we need to sum up all the elements $m_{kl} \in \mathbb{C}$ in the matrix $M(\omega_i)$ and minimize the objective function J defined as:

$$J = \min_{\varphi} \sum_{k=1}^{n_u} \sum_{l=1}^{n_u-1} |m_{kl}|. \tag{3.12}$$

Because we parameterize the input mode shape $T'_{u,1}$ with the sphere coordinates $\varphi = [\varphi_1, \varphi_2, \dots, \varphi_{n_u-1}]$, this will lead to a non-linear multi-variable optimization problem, and Matlab toolboxes such as Genetic Algorithm Toolbox can be used to find the optimum solution for ϕ.

Step 2: Obtain the modal filter for the mode to be controlled :
According to Definition 1, the efficiency factor η of the coordinate transformation vectors $T_{u,i}$ and $T_{y,i}$ on the original system $G(s)$ can be represented as:

$$\eta = \left\| T_{y,i}^T G(s) T_{u,i} \right\|_{\mathcal{H}_2}. \tag{3.13}$$

So the following optimization problem can be formulated to obtain the optimum transformation vectors with unit length $T_{u,i}$ and $T_{y,i}$ [18]:

$$\begin{aligned} \max_{T_{u,i}, T_{y,i}} \quad & \left\| T_{y,i}^T G(s) T_{u,i} \right\|_{\mathcal{H}_2} \\ \text{subject to} \quad & \left\| T_{u,i} \right\|_2 = 1 \\ & \left\| T_{y,i} \right\|_2 = 1 \\ & T'_u T_{u,i} = 0 \\ & T'_y T_{y,i} = 0, \end{aligned} \tag{3.14}$$

The last two conditions in Equation 3.14 ensure that the optimum vectors $T_{u,i}$ and $T_{y,i}$ we obtained are orthogonal to the direction of the modes we want to isolate. Therefore we can achieve both mode decoupling and have maximum controllability and observability of the targeted mode.

To transform the multi-variable optimization problem into a single variable, the Lemma 1 can be used:

$$\left\| T_{y,i}^T G(s) T_{u,i} \right\|_{\mathscr{H}_2} = \left| T_{y,i}^T G(\omega_i) T_{u,i} \right| \sqrt{\omega_n \zeta}. \tag{3.15}$$

Looking at the right side of the equation, the second term $\sqrt{\omega_n \zeta}$ only relates to the modal property of the mode so that it can be taken out of the optimization problem. For the first term $\left| T_{y,i}^T G(\omega_i) T_{u,i} \right|$, it can be considered as the complex number z in Definition 2, so we can replace the process of finding the modules of complex number z, by a single variable optimization problem:

$$\left| T_{y,i}^T G(\omega_i) T_{u,i} \right| = \max_{\theta} \; T_{y,i}^T f(\theta) T_{u,i}, \tag{3.16}$$

where $f(\theta)$ is shown in Definition 2. Therefore, we can reduce the total optimization variables needed from $n_u + n_y$ to only one,

Then, to enable the decoupling constraint in Equation 3.14, we need to constraint the vectors $T_{u,i}$ and $T_{y,i}$ in the null space of matrices T_u' and T_y' respectively. This can be achieved by transforming the original vectors $T_{u,i}$ and $T_{y,i}$ into the new vectors $\hat{T}_{u,i}$ and $\hat{T}_{y,i}$ using the N_u and N_y calculated in Equation 3.8 and 3.9:

$$\begin{aligned} T_{u,i} &= N_u \hat{T}_{u,i} \\ T_{y,i} &= N_y \hat{T}_{y,i}. \end{aligned} \tag{3.17}$$

Therefore, by replacing the old variables $T_{u,i}$ and $T_{y,i}$ with new variables $\hat{T}_{u,i}$ and $\hat{T}_{y,i}$, Equation 3.16 is now augmented with the mode decoupling constraint and can be rewritten as:

$$\begin{aligned} \left| T_{y,i}^T G(\omega_i) T_{u,i} \right| &= \left| \hat{T}_{y,i}^T N_y^T G(\omega_i) N_u \hat{T}_{u,i} \right| \\ &= \max_{\theta} \; \hat{T}_{y,i}^T N_y^T F(\theta) N_u \hat{T}_{u,i}. \end{aligned} \tag{3.18}$$

Therefore, the original problem in Equation 3.14 can be considered as the following optimization problem:

$$\begin{aligned} \max_{T_{u,i}, T_{y,i}} \left| T_{y,i}^T G(\omega_n) T_{u,i} \right| &= \max_{\hat{T}_{u,i}, \hat{T}_{y,i}} \left| \hat{T}_{y,i}^T N_y^T G(\omega_n) N_u \hat{T}_{u,i} \right| \\ &= \max_{\hat{T}_{u,i}, \hat{T}_{y,i}} \max_{\theta} \left(\hat{T}_{y,i}^T N_y^T F(\theta) N_u \hat{T}_{u,i} \right) \\ &= \max_{\theta} \max_{\hat{T}_{u,i}, \hat{T}_{y,i}} \left(\hat{T}_{y,i}^T N_y^T F(\theta) N_u \hat{T}_{u,i} \right). \end{aligned} \tag{3.19}$$

To solve the optimization in Equation 3.19, we first need to find the optimum θ^* in the first optimization step. After the optimum θ^* has been computed, because vectors $\hat{T}_{u,i}$ and $\hat{T}_{y,i}$ both have the unit length, the second optimization problem

of Equation 3.19 can be seen as finding the maximum singular value σ_{max} of the matrix $N_y^T F(\theta^*) N_u$ [18]:

$$\max_{\hat{T}_{u,i}, \hat{T}_{y,i}} \hat{T}_{y,i}^T \left(N_y^T F(\theta^*) N_u \right) \hat{T}_{u,i} = \left\| N_y^T F(\theta^*) N_u \right\|_2 = \sigma_{max}. \tag{3.20}$$

Therefore, the optimum vectors $\hat{T}_{u,i}$ and $\hat{T}_{y,i}$ can be directly obtained by using the Singular Value Decomposition (SVD) on matrix $N_y^T F(\theta^*) N_u$:

$$N_y^T F(\theta^*) N_u = \begin{bmatrix} \hat{T}_{y,i} & \dots \end{bmatrix} \begin{bmatrix} \sigma_{\max} & 0 \\ 0 & \dots \end{bmatrix} \begin{bmatrix} \hat{T}_{u,i} & \dots \end{bmatrix}^T, \tag{3.21}$$

where the $\hat{T}_{u,i}$ and $\hat{T}_{u,i}$ are the right-singular vectors and left-singular vectors, respectively.

After that, we can recover the actual vectors $T_{u,1}$ and $T_{y,i}$ by again using Equation 3.17:

$$T_{u,i} = N_u \hat{T}_{u,i}$$
$$T_{y,i} = N_y \hat{T}_{y,i}.$$

To conclude Section 3.4, the algorithm can be summarized as follow: First, we need to calculate the null space N_u and N_y in which the dynamics of other modes are isolated from the targeted mode, and this can be obtained by solving the first optimization problem in Equation 3.12. Second, we need to calculate the modal transformation vector T_u and T_y, which give the maximum observability and controllability in terms of the $\mathscr{H}_2$ norm over the targeted mode, and these vectors can be obtained by solving the second optimization problem in Equation 3.19.

After we obtain the vectors $T_{u,i}$ and $T_{y,i}$, all the actuator signals U and sensor signals Y can be combined and distributed so that only the targeted mode can be actuated and observed by the SISO controller. As a result, any SISO Active Vibration controller can now be used as the modal controller.

3.5. DATA-BASED MODAL ACTIVE DAMPING — EXPERIMENTS

3.5.1. DESCRIPTION OF EXPERIMENTAL SETUP

In order to validate the performance of the proposed data-based filter, a vertically clamped cantilever made up of aluminum will be used to represent the lightweight, flexible system. The complete system consists of a flexible beam with four collocated piezoelectric patches acting as actuators and sensors. A piezoelectric stack actuator at the root of the beam will be used to generate the disturbance signal, and an accelerometer will be placed at the tip of the beam to measure the vibration amplitude. The accelerometer and the stack actuator will be used as the performance channel to evaluate the damping performance. For real-time implementation, the National Instruments Compact RIO FPGA Module is used to obtain the sensor outputs and compute and send the control signal to the voltage amplifier BD-300 to drive the piezoelectric actuator. The final assembled experimental setup and its illustrative diagram are shown in Figure 3.5.

To obtain the MIMO FRD model of the system, a swept sine signal from 1 Hz to 1000 Hz is performed on each piezoelectric actuator to excite the system. And to collect each sensor output, a sampling rate of 10 kHz for the FPGA Module is chosen to provide a more accurate reconstruction of the frequency response below 1000 Hz.

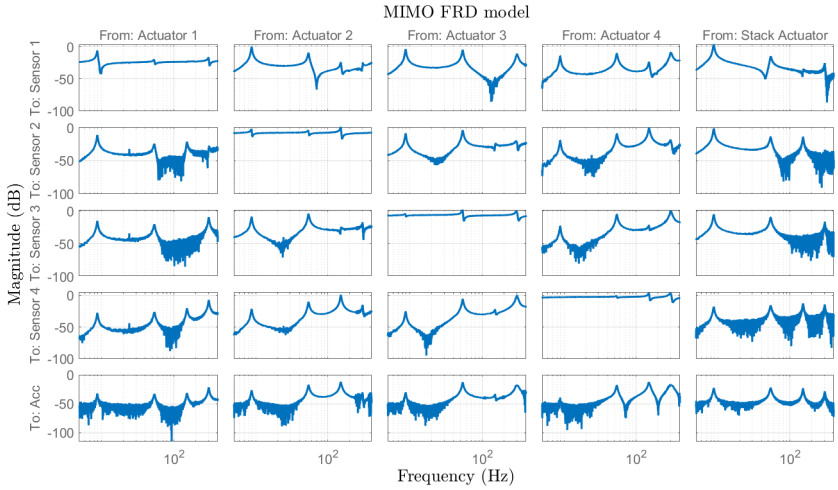

Figure 3.4.: MIMO frequency response function obtained from the experimental setup

After obtaining the time domain data, the Matlab System Identification Toolbox is used to obtain the complete five-by-five MIMO FRD model, which also includes the aforementioned performance channel. The bode plot of this FRD model is shown in Figure 3.4, and it will be used to design the filter in Section 3.5.2.

3.5.2. FILTER IMPLEMENTATION

From the experimental data, five resonance peaks are clearly visible within the identified frequency range, which is located at 8.68, 53.2, 149, 296, and 485 Hz, respectively. With the identified resonance frequency, we can directly use the MIMO FRD model in the proposed algorithm in Section 3.4 to compute the vectors $T_{u,i}$ and $T_{y,i}$. Because there are a total of four collocated piezoelectric patches in the system, we can choose to isolate any of these five modes from the other three modes. So, to validate the performance of the filter on the real experimental data, the goal is to dampen the third mode at 53.2 Hz, and the filter should isolate it from the modes at 8.68, 53.2, and 296 Hz.

Using the acquired data and the method described in section 3.4, the vectors $T_{u,3}$ and $T_{y,3}$ can be computed as:

$$T_{u,3} = [0.49; -0.74; 0.38; 0.26],$$

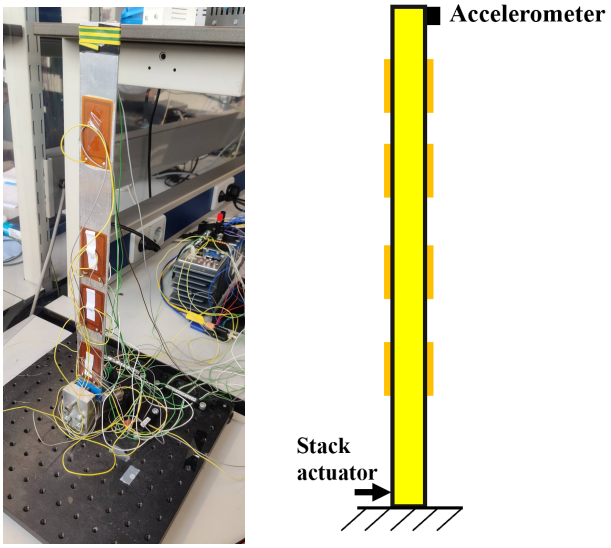

(a) The assembled setup

(b) Illustration of experimental setup

Figure 3.5.: The experimental setup

and

$$T_{y,3} = [0.16; -0.76; 0.51; 0.26].$$

In Figure 3.6, we can evaluate the performance of the computed vectors $T_{u,3}$ and $T_{y,3}$ in the open loop and compare it with the aforementioned performance channel. In the upper magnitude of Figure 3.6, we can observe there are four peaks visible in the performance channel, but we can only observe one peak at 53.2 Hz in the filter channel. The flat line outside of the third resonance means the modes at 8.68, 53.2, and 296 Hz are completely isolated from the third mode. Also, we can examine the phase plot to have the same conclusion: in the performance channel, the phase is dropping every $-180°$ after each resonance, but in the filter channel, the phase is only dropping to nearly $-180°$ for the third mode, and within the considered range of frequencies, the phase always stays at $0°$ line and we can not observer any phase drop due to resonance, which indicates nearly perfect isolation the non-targeted modes. And the phase is only slightly dropping as the frequency increase because of the time delay in the system.

3.6. CONCLUSION

In this paper, a novel data-based modal control method is introduced, aiming at dampening the harmful flexible modes using a large number of actuators and sensors. The proposed method has been verified using the MIMO non-parametric frequency response obtained from the experimental setup, which shows nearly

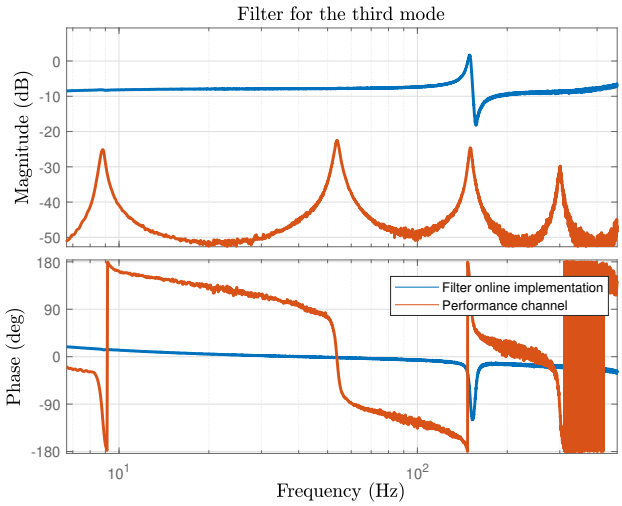

Figure 3.6.: Online implementation of $T_{u,3}$ and $T_{y,3}$

perfect isolation of the mode of interest. Then, a SISO controller using all available actuators and sensors can be implemented to dampen this mode, which greatly reduces tuning effort compared to the decentralized control architecture.

REFERENCES

[1] R. M. Schmidt, G. Schitter, A. Rankers, and J. van Eijk. *The design of high performance mechatronics: High-tech functionality by multidisciplinary system integration: 2nd revised edition*. IOS Press, Jan. 2014, pp. 1–901. ISBN: 9781614993681. DOI: 10.3233/978-1-61499-368-1-I.

[2] K. Verbaan, N. Rosielle, and M. Steinbuch. "Bandwidth increase by shaping the plant in combination with the controller - The role of damping in positioning tables". In: *Proceedings of the IEEE International Conference on Control Applications* (2013), pp. 1099–1104. DOI: 10.1109/CCA.2013.6662898.

[3] L. Meirovitch and H. Baruh. "CONTROL OF SELF-ADJOINT DISTRIBUTED-PARAMETER SYSTEMS." In: *AIAA Paper* (1980), pp. 1–10. ISSN: 01463705. DOI: 10.2514/6.1980-1707.

[4] P. de Bruin. *Input and state estimation for compliant motion stages: Estimating modal contribution for guidance flexures*. 2022.

[5] J. Watchi, B. Ding, G. Zhao, and C. Collette. "Study of MIMO Control Laws for Seismic Isolation of Flexible Payload". In: *2019 IEEE 7th International Conference on Control, Mechatronics and Automation, ICCMA 2019* (Nov. 2019), pp. 248–252. DOI: 10.1109/ICCMA46720.2019.8988713.

[6] D. Vaes, J. Swevers, and P. Sas. "Optimal decoupling for MIMO-controller design with robust performance". In: (May 2004), pp. 4601–4606. DOI: 10.23919/ACC.2004.1384036.

[7] Q. Tang, F. Guo, T. Huang, K. Yang, Y. Zhu, and M. Li. "Modal-Decomposition-Dependent State-Space Modeling and Modal Analysis of a Rigid-Flexible, Coupled, Multifreedom Motion System: Theory and Experiment". In: *Shock and Vibration* 2020 (2020). ISSN: 10709622. DOI: 10.1155/2020/8859222.

[8] J. Stoev, J. Ertveldt, T. Oomen, and J. Schoukens. "Tensor methods for MIMO decoupling and control design using frequency response functions". In: *Mechatronics* 45 (Aug. 2017), pp. 71–81. ISSN: 0957-4158. DOI: 10.1016/J.MECHATRONICS.2017.05.009.

[9] T. Oomen. "Advanced motion control for precision mechatronics: control, identification, and learning of complex systems". In: *IEEJ Journal of Industry Applications* 7.2 (Jan. 2018), pp. 127–140. ISSN: 2187-1094. DOI: 10.1541/IEEJJIA.7.127.

[10] T. Oomen, R. Van Herpen, S. Quist, M. Van De Wal, O. Bosgra, and M. Steinbuch. "Next-generation wafer stage motion control: Connecting system identification and robust control". In: *Proceedings of the American Control Conference* (2012), pp. 2455–2460. ISSN: 07431619. DOI: 10.1109/ACC.2012.6314685.

[11] M. Gopal and M. Mallur. *A comparative study on distributed active damping of flexible systems*. 2020.

[12] T. van der Graaf. *Active Vibration Control: using over-sensing and over-actuation*. 2021.

[13] J. Holterman and T. J. de Vries. "Active damping based on decoupled collocated control". In: *IEEE/ASME Transactions on Mechatronics* 10.2 (Apr. 2005), pp. 135–145. ISSN: 10834435. DOI: 10.1109/TMECH.2005.844702.

[14] B. Babakhani. "Active Damping of Vibrations in High-Precision Motion Systems". PhD thesis. Enschede, The Netherlands: University of Twente, Nov. 2012. ISBN: 9789036534642. DOI: 10.3990/1.9789036534642.

[15] A. Rankers. "Machine dynamics in mechatronic systems, an engineering approach". PhD thesis. University of Twente, June 1997.

[16] R. Hoogendijk. "Control of flexible motion systems using frequency response data". PhD thesis. Eindhoven University of Technology, 2014. ISBN: 9789038636481. DOI: 10.6100/IR774666.

[17] S. Skogestad and I. Postlethwaite. *Multivariable Feedback Control: Analysis and Design*. john Wiley & sons, 1996.

[18] V. Promotionsausschuss, M. Pusch, and S. Martin. "Blending of inputs and outputs for modal control of aeroelastic systems". PhD thesis. Technische Universität Hamburg, 2020.

[19] M. Pusch and D. Ossmann. "H2 Optimal Blending of Inputs and Outputs for Modal Control". In: *IEEE Transactions on Control Systems Technology* 28.6 (Nov. 2020), pp. 2744–2751. ISSN: 15580865. DOI: 10.1109/TCST.2019.2942281.

[20] M. Pusch. "Aeroelastic mode control using H2-optimal blends for inputs and outputs". In: *AIAA Guidance, Navigation, and Control Conference, 2018* (Jan. 2018). DOI: 10.2514/6.2018-0618.

[21] D. Vaes, J. Swevers, and P. Sas. "Optimal decoupling to simplify and improve multivariable control design". In: *Mediterranean Journal of Measurement and Control* 2.2 (Oct. 2006), pp. 48–62. URL: https://lirias.kuleuven.be/1566696.

[22] R. F. Heertjes, M. F. Molengraft, M. J. G. Van De, and M. Steinbuch. "Directional notch filter for motion control of flexible structures". In: *Mechatronics* 24.6 (2014), p. 632. DOI: 10.1016/j.mechatronics.2014.01.011.

4

DISCUSSION

The following sections discuss additional aspects of the method with the aim of providing further insights into the method and motivating future developments.

4.1. EXPERIMENTAL STUDY

FILTER IMPLEMENTATION FOR OTHER MODES

In chapter 3, we have demonstrated the proposed data-based modal control method can perfectly isolate the third mode from the rest of the dynamics in the frequency range of interests. In this section, we want to demonstrate the applicability of this method by applying it to the other modes.

In Figure 4.1, the second mode at 53.2 Hz is isolated from the modes at 8.68, 149, and 296 Hz. The vectors $T_{u,2}$ and $T_{y,2}$ is computed as:

$$T_{u,2} = [-0,74; 0,40; 0,38; 0,35],$$

and

$$T_{y,2} = [-0,44; 0,73; 0,27; -0,43].$$

In Figure 4.1, from the Bode magnitude plot, we can see the flat line outside of the second resonance, which indicates good isolation of the second mode. From the phase plot, we can only observe a significant phase drop at around 50 Hz. But for the first mode at around 8 Hz, we could see a negligible phase drop for a few degrees, and for the third mode at around 149 Hz, we could see a very small phase lead which does not correspond to the plant's collocated behavior.

In Figure 4.2, the open loop response of filter $T_{u,3}$ and $T_{y,3}$ is plotted, which has been described in detail in section 3.5.2.

In Figure 4.3, the fourth mode at 296 Hz is isolated from the modes at 8.68, 149, and 53.2 Hz The vectors $T_{u,4}$ and $T_{y,4}$ is computed as:

$$T_{u,4} = [-0,37; 0,59; -0,55; 0,44],$$

and

$$T_{y,4} = [-0,08; 0,57; -0,68; -0,42].$$

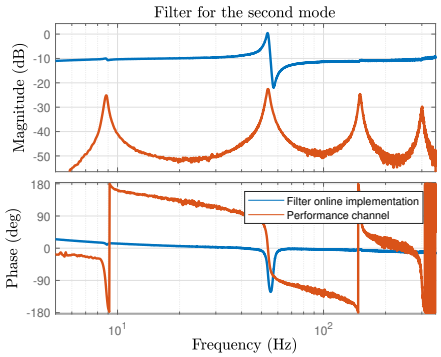

Figure 4.1.: Online implementation of $T_{u,2}$ and $T_{y,2}$

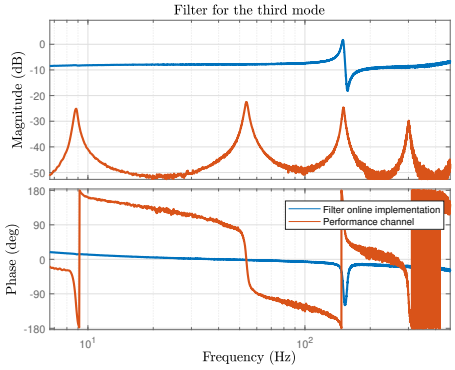

Figure 4.2.: Online implementation of $T_{u,3}$ and $T_{y,3}$

In Figure 4.3, we have the same conclusion for the performance of vectors $T_{u,4}$ and $T_{y,4}$. From Figure 4.3, before the fourth mode at 296 Hz, we can see the flat line both in the magnitude plot and the phase plot, which indicates perfect isolation of the first three modes.

In Figure 4.4, the first mode at 8 Hz is isolated from the modes at 149 and 53.2 Hz. The reason for this is that the filters $T_{u,1}$ and $T_{y,1}$ are designed based on the initial setup with only three collocated piezoelectric patches, so the maximum number of modes the filter can isolate is two. But from the bode plot, we can also conclude this filter is able to isolate the second and the third mode from the first one.

ACTIVE DAMPING CONTROLLER

After we have examined the performance of the vectors $T_{u,3}$ and $T_{y,3}$ in Section 3.5.2 and concluded it could achieve nearly perfect mode decoupling, we can then design a SISO controller for all four collocated piezoelectric patches just for the targeted mode. Be-

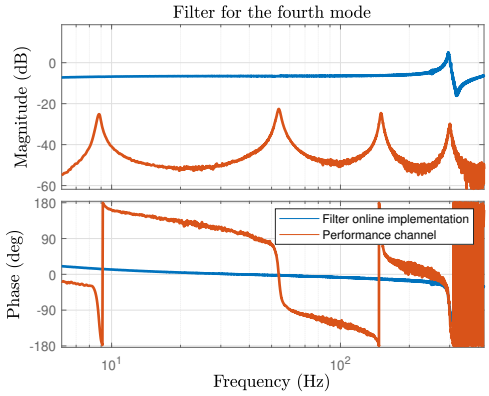

Figure 4.3.: Online implementation of $T_{u,4}$ and $T_{y,4}$

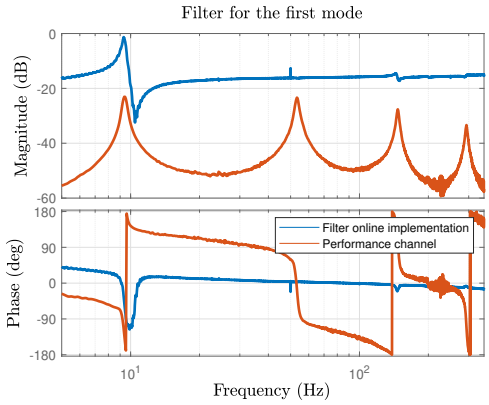

Figure 4.4.: Online implementation of $T_{u,1}$ and $T_{y,1}$

cause the cantilever beam is a continuum system, there is an infinite number of modes in the system. But we only have a total of four collocated patches, so we can only isolate up to the fourth mode as explained in Section 3.4. To avoid the excitation of higher-order modes that we can not isolate, we would use a controller with low-pass characteristics, such as Positive Position Feedback (PPF), to dampen the targeted mode.

The transfer function of the PPF controller $C(s)$ is given as follows:

$$C(s) = \frac{-g\omega_f^2}{s^2 + 2\zeta_f\omega_f s + \omega_f^2}, \tag{4.1}$$

where g, ω_f, and ζ_f are the tuning parameters and represent the gain factor, corner frequency, and damping ratio, respectively.

To implement the controller, we set the corner frequency $\omega_f = 53.2$ Hz, which is the

resonance frequency of the third mode, and the gain and the damping ratio are tuned to be $g = 0.25$ and $\zeta_f = 0.2$.

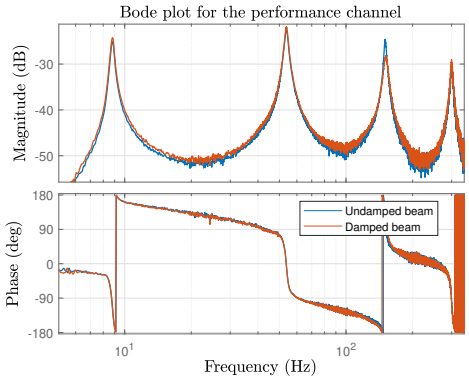

Figure 4.5.: Frequency response of the performance channel

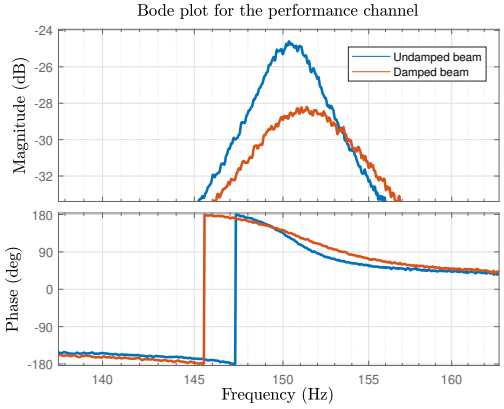

Figure 4.6.: Zoomed in view at the resonance for Figure 4.5

To evaluate the damping performance, we can compare the undamped plant and the damped plant in the performance channel, which is from the piezoelectric stack actuator at the base to the accelerometer at the tip. In Figure 4.5, the two frequency responses, the damped plant, and the undamped plant, are plotted.

4.2. SIMULATION

In this section, the initial simulation to study the algorithm is shown. The system is the same as the experimental setup: four collocated piezoelectric patches attached to an aluminum beam with the same dimension and with a piezo stack actuator and an accelerometer acting as the performance channel. But in the simulation, only four flexible modes are included in the system. Because there are no higher-order modes after the fourth mode, we could observe the -2 slope at the high frequency. From Figure 4.7, we can see that in the offline simulation, filter $T_{u,3}$ and $T_{y,3}$ can isolate the third mode from the system. What is more interesting is the pole-zero map in Figure 4.8, and from this figure, we can conclude that what the algorithm really did is to place the zero at the location of the pole that we want to isolate, and it achieved that only using the information of the frequency response without obtaining the actual pole location from the parametric model.

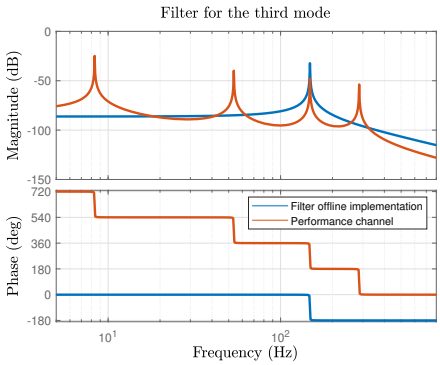

Figure 4.7.: Offline simulation of $T_{u,3}$ and $T_{y,3}$

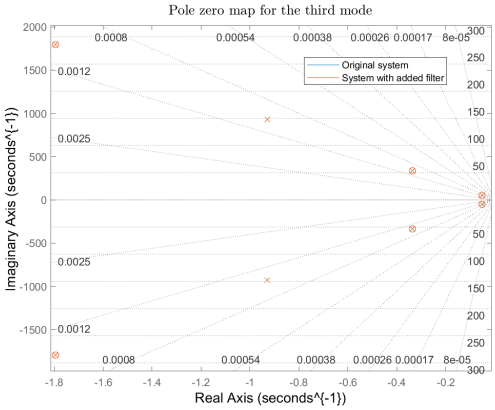

Figure 4.8.: Pole zero map of $T_{u,3}$ and $T_{y,3}$

5

CONCLUSIONS

5.1. CONCLUSION

In this thesis, a novel data-based modal control scheme for active damping was developed. This was motivated by the increasing requirement for speed and precision in the mechatronics system, and a solution is needed to dampen the flexible mode that is limiting the maximum achievable bandwidth.

After the literature study, it was concluded that a modal control method is needed to improve the current decentralized control architecture. Another requirement is that this modal control method should be based on the frequency response function, which can be easily obtained, and this will allow the possibility to circumvent the time-consuming process of obtaining an accurate parametric model.

In this thesis, the aforementioned requirement is fulfilled by developing an optimization algorithm that allows us to compute a set of vectors that combine all the sensor signals and redistribute all the actuator signals in such a way that only a single flexible mode is made controllable and observable. In this way, the dynamics of other modes are filtered out of the active vibration control loop.

This method was then validated experimentally on a cantilever beam with four collocated placed transducers. The experiment shows that the computed vectors can perfectly isolate the targeted mode from the rest of the dynamics. Then, a SISO active vibration controller can be implemented to dampen the targeted mode using all available sensors and actuators.

5.2. RECOMMENDATION

In this section, recommendations for future work is given:

- In section 3, we have validated the proposed method on the experiment setup: after we have obtained the frequency response function, the proposed method can make the specific flexible mode both uncontrollable and unobservable. However, in practice, making one mode either uncontrollable or unobservable should be sufficient to let this mode disappear from the frequency response. In future work, one possible direction could be to investigate what is the optimum arrangement for the unobservability and uncontrollability of a mode

such that we could cover a wider range of frequencies with the same amount of actuators and sensors.

- Another possible direction is to investigate how to use the zero calculated in the algorithm to have the maximum reachable damping. In [1], the authors have proven that for a lightly damped MIMO system with collocated transducers, a low authority control law will have the property that the maximum achievable damping for a mode is proportional to the distance between the pole and the transmission zero. This may imply that other than using the zeros to make the mode unobservable and uncontrollable, the zeros can also be placed in a smart way so that the maximum achievable damping for the active vibration controller is increased. And this naturally begs the question of how we can measure the distance between a pole and a transmission zero in the system when this system is described only using frequency response function. If this distance can be calculated, or a value that is proportional to this quantity is obtained, how can the maximizing of this value be incorporated into the existing optimization scheme?

REFERENCES

[1] D. Piron, S. Pathak, A. Deraemaeker, and C. Collette. “On the link between pole-zero distance and maximum reachable damping in MIMO systems”. In: *Mechanical Systems and Signal Processing* 181 (Dec. 2022), p. 109519. ISSN: 0888-3270. DOI: 10.1016/J.YMSSP.2022.109519.

A

EXPERIMENT

In Appendix A, how to use Compact Rio FPGA Module with Labview for real-time implementation will be explained.

A.1. LABVIEW PROJECT

In Figure A.1, all the Labview files and the FPGA hardware is shown. For the FPGA module, we use two FPGA analog inputs NI9263, to collect the outputs of the piezoelectric sensors and one FPGA analog input NI 9201, to send the control signal to the piezoelectric actuators via the amplifier. The files that are most relevant for the implementation are the Host.vi, RTMain.vi, and the FPGA.vi highlighted in Figure A.1.

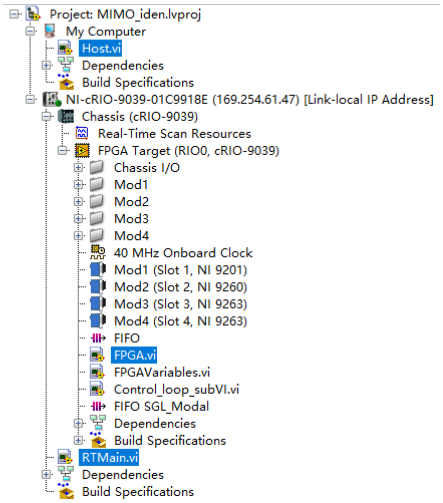

Figure A.1.: Project

The FPGA.vi file can be considered as the real-time control loop: the FPGA module collects all the sensor data and processes them based on the instruction in the FPGA.vi

A

file and send the control signal to the FPGA output ports. It is worth noting that any modification in the FPGA.vi file will result in the recompiling of the file, which will take 20 to 40 minutes depending on the file size.

And what makes the FPGA an attractive option for real-time implementation is that each loop can run parallel, so the delay caused by the computation is reduced significantly compared to the MCU board, such as TI2000. In the following figure, we will show the most important control loop in the FPGA.vi file.

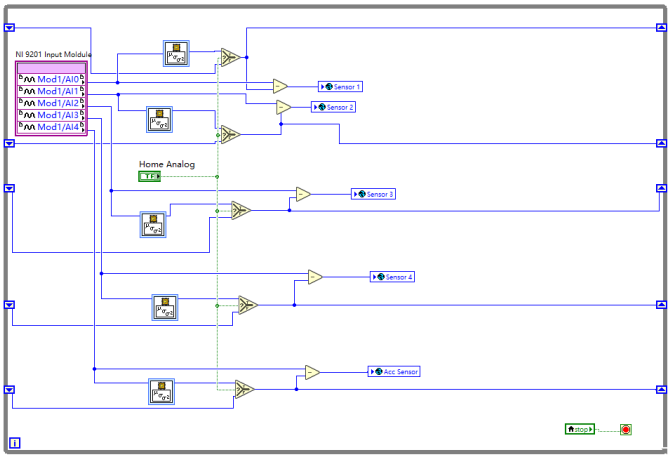

Figure A.2.: Data collection loop

In Figure A.2, the data collection loop is shown. The data is collected from AI0 to AI5, and it is sent to the global variable, such as Sensor 1 and Sensor 2. The block between them can be used to find the new zero point of the signal when the sensor needs to be re-calibrated.

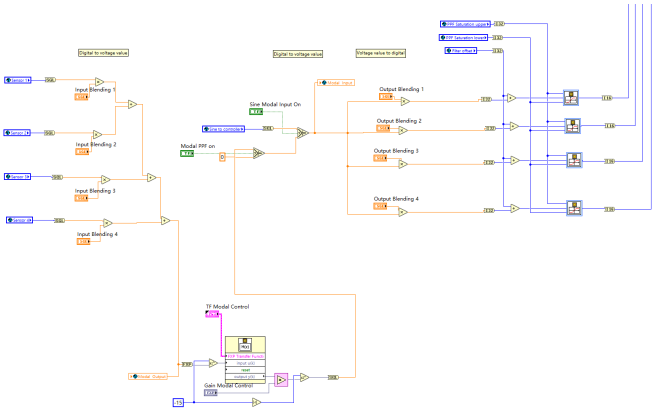

Figure A.3.: Data process loop

In Figure A.3, the data process loop is shown. After the data is collected and stored in the global variable, the data process loop will compute the output to the actuator based on the specified control algorithm.

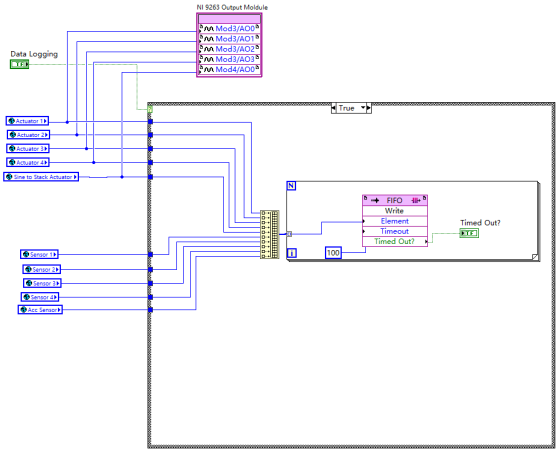

Figure A.4.: Data storage loop

In Figure A.4, the data storage loop is shown. All of the data will be sent to the computer via a FIFO block. These data can be later processed in Matlab.

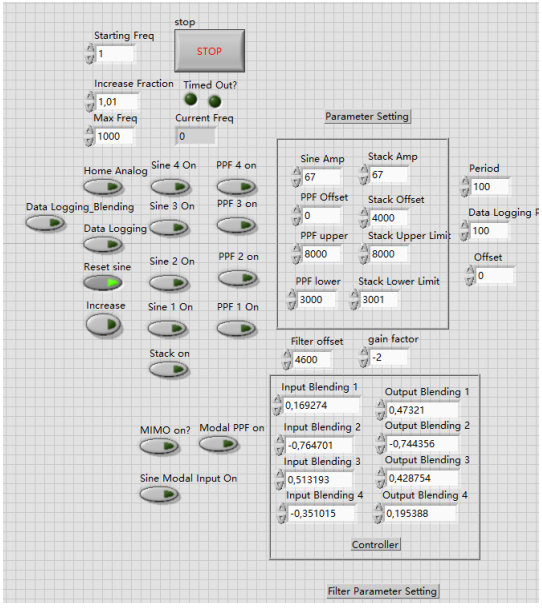

Figure A.5.: RTMain control panel

We have mentioned in this section before that any modification in the FPGA.vi file will result in a re-compilation time of around 20 to 40 minutes. So, to shorten the waiting time, any possible changes of the parameter will be put into the RTMain.vi. The control panel of this file is shown in A.5. We can change the control parameter while the FPGA.vi is running, such as the on and off switch, and the parameter for the Input Blending and Output Blending.

After that, we need to store all of the useful data in the computer, such as the sensor outputs and the actuator input. This is done in the Host.vi file. The front panel and the back panel of this file are shown in Figure A.6 and Figure A.7. In the front panel, we can monitor the data while the FPGA is running. And in the back panel, how the data is sent to the host computer via FIFO block is shown.

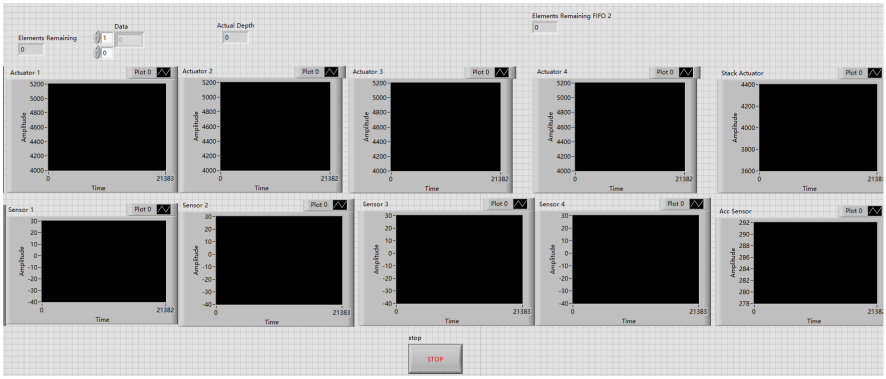

Figure A.6.: Host.vi front panel

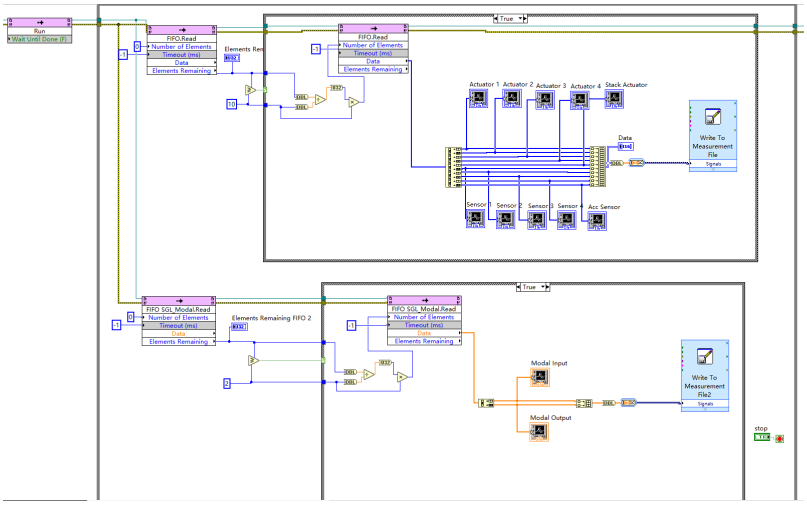

Figure A.7.: Host.vi back panel

Finally, the data collected in the Labview can be imported into Matlab for post-processing. In Figure A.8, we show the correct setting for importing the date to Matlab.

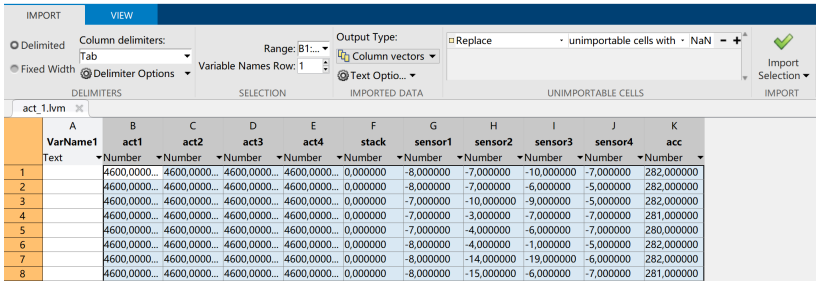

	A	B	C	D	E	F	G	H	I	J	K
	VarName1	act1	act2	act3	act4	stack	sensor1	sensor2	sensor3	sensor4	acc
	Text	Number	Number	Number	Number	Number	Number	Number	Number	Number	Number
1		4600,0000...	4600,0000...	4600,0000...	4600,0000...	0,000000	-8,000000	-7,000000	-10,000000	-7,000000	282,000000
2		4600,0000...	4600,0000...	4600,0000...	4600,0000...	0,000000	-8,000000	-7,000000	-6,000000	-5,000000	282,000000
3		4600,0000...	4600,0000...	4600,0000...	4600,0000...	0,000000	-7,000000	-10,000000	-9,000000	-5,000000	282,000000
4		4600,0000...	4600,0000...	4600,0000...	4600,0000...	0,000000	-7,000000	-3,000000	-7,000000	-7,000000	281,000000
5		4600,0000...	4600,0000...	4600,0000...	4600,0000...	0,000000	-7,000000	-4,000000	-6,000000	-7,000000	280,000000
6		4600,0000...	4600,0000...	4600,0000...	4600,0000...	0,000000	-8,000000	-4,000000	-1,000000	-5,000000	282,000000
7		4600,0000...	4600,0000...	4600,0000...	4600,0000...	0,000000	-8,000000	-14,000000	-19,000000	-6,000000	282,000000
8		4600,0000...	4600,0000...	4600,0000...	4600,0000...	0,000000	-8,000000	-15,000000	-6,000000	-7,000000	281,000000

Figure A.8.: Import data in Matlab

B

MATLAB CODE

The Matlab code for the proposed method is listed below. The input is the frequency response data (FRD) collected from the simulation model or the experiment.

```
%% Setting Section
clear
clc

 load('SYS.mat');
 load('filter_onine_identification.mat');
 load('Gnew.mat');

 load('H_0601');
 load('BV1');
 load('BV2');
 load('BV3');
 load('BV4');

 load('H_full_FRD');

 load('PPF_off');
 load('PPF_on');


s= tf('s');

SYS.H = H(1:4,1:4);
SYS.A=A;
SYS.B=B;
SYS.C=C;
SYS.D=D;
SYS.Cmodal=Cmodal;
SYS.Nmodes=Nmodes;
```

```
SYS.omega2=omega2;

SYS.ky=[];
SYS.ku=[];
SYS.sys_ss=[];
SYS.k=[];
SYS.sys_fb=[];
SYS.Htf_nest =[];
SYS.InputModeShape = [];
SYS.OutputModeShape = [];
SYS.NumOfPatch = 4;

SYS.wn =[];
SYS.wn1 =[];

% Setting
BVSetting.IsModeDecoupled = true;
BVSetting.DampedMode = 1;


%%  Main Section
SYS1 = SYS;
SYS2 = SYS;
SYS3 = SYS;
SYS4 = SYS;

SYS1.wn = 2*pi*[ 8.68 53.2  149 296];
SYS1.wn1 = 2*pi*[ 8.68 53.2  149 296];
SYS1 = getInMS(SYS1);
SYS1 = getOutMS(SYS1);
SYS1 =FindBV(SYS1);

SYS2.wn = 2*pi*[ 53.2 8.68  149 296];
SYS2.wn1 = 2*pi*[ 53.2 8.68  149 296];
SYS2 = getInMS(SYS2);
SYS2 = getOutMS(SYS2);
SYS2 =FindBV(SYS2);

SYS3.wn = 2*pi*[   149 53.2 8.68 296];
SYS3.wn1 = 2*pi*[  149 53.2 8.68 296];
SYS3 = getInMS(SYS3);
SYS3 = getOutMS(SYS3);
SYS3 =FindBV(SYS3);

SYS4.wn = 2*pi*[ 296 53.2 8.68  149 ];
```

```
SYS4.wn1 = 2*pi*[ 296 53.2 8.68  149 ];
SYS4 = getInMS(SYS4);
SYS4 = getOutMS(SYS4);
SYS4 =FindBV(SYS4);


%%
opts = bodeoptions('cstprefs');
opts.MagUnits = 'db';
opts.XLim= [5 0.45e3];
opts.Grid = 'on';
opts.PhaseWrapping = 'on';
opts.PhaseWrappingBranch = -180;
opts.PhaseVisible = 'on';
opts.Title.String = '';
opts.Title.Interpreter = 'latex';
opts.XLabel.Interpreter = 'latex';
opts.YLabel.Interpreter = 'latex';
opts.XLabel.FontSize = 13;
opts.YLabel.FontSize = 13;
opts.Title.FontSize = 13;


 figure()
 bode( -SYS1.ky' * SYS1.H * SYS1.ku,-BV1, opts)
 legend('Offline filter','Online filter')
 title('Filter for the first mode')

 figure()
 bode( -SYS2.ky' * SYS2.H * SYS2.ku,-BV2, opts)
 legend('Offline filter','Online filter')
 title('Filter for the second mode')

  figure()
  opts.XLim= [5 0.35e3];
 bode(-BV2,PPF_off, opts)
 legend('Filter online implementation','Performance
    channel')
 title('Filter for the second mode')
 h = findobj(gcf,'type','line');
set(h,'linewidth',2);


 figure()
  opts.XLim= [5 0.35e3];
```

```
 bode(-BV3,PPF_off, opts)
 legend('Filter online implementation','Performance
    channel')
 title('Filter for the third mode')
 h = findobj(gcf,'type','line');
set(h,'linewidth',2);

 figure()
 bode( -SYS4.ky' * SYS4.H * SYS4.ku,-BV4, opts)
 legend('Offline filter','Online filter')
 title('Filter for the fourth mode')

   figure()
  opts.XLim= [5 0.35e3];
 bode(-BV4,PPF_off, opts)
 legend('Filter online implementation','Performance
    channel')
 title('Filter for the fourth mode')
 h = findobj(gcf,'type','line');
set(h,'linewidth',2);

figure()
bode(PPF_off,PPF_on,opts)
legend('Undamped beam','Damped beam')
title('Bode plot for the performance channel')
h = findobj(gcf,'type','line');
set(h,'linewidth',2);

figure()
opts.PhaseVisible = 'off';
bode(H,opts)
title('MIMO FRD model')
h = findobj(gcf,'type','line');
set(h,'linewidth',1.5);




%% Design PPF
Fs = 1e4;
ts = 1/Fs;
W= 149*2*pi;
g = 0.05;
eta=0.10;
k=1/0.398;
```

```
sign = 1;
PPF = sign*tf([1*k*g],[1/W^2 2*eta/W 1]);%
PPFd = c2d(PPF,ts,'tustin');


%% Coefficient for Labview
PPF_numd = cell2mat(PPFd.Numerator);
PPF_dend = cell2mat(PPFd.Denominator);
gain = 1;
Labview_PPF_num = -1 * gain * fliplr(PPF_numd)  % one -
    in system, no - in fb, one - in PPF = +
Labview_PPF_den = fliplr(PPF_dend)


%% Function Seciton
function [SYS]=FindBV(SYS)


BVSetting=SYS.BVSetting;
wn = SYS.wn;



n = BVSetting.DampedMode;
wn1 = wn(n);
M = SYS.H;




if BVSetting.IsModeDecoupled == false

[reZ,imZ] = nyquist(M,wn1);
bnd_min= 0; bnd_max = pi;
F = @(phi) -norm(  (reZ * cos(phi) + imZ * sin(phi))  ,2)
    ;
phi_star = fminbnd(F,bnd_min,bnd_max) ;

Fmat =  (reZ * cos(phi_star) + imZ * sin(phi_star)) ;
[ky_mat,~,ku_mat] = svd(Fmat);
ku_true = ku_mat(:,1);
ky_true = ky_mat(:,1);
effi = norm(ky_true' * M * ku_true, 2)/norm(M ,2) ;

elseif BVSetting.IsModeDecoupled == true
```

```
205
206 B1 = SYS.InputModeShape(:,1);
207 B2 = SYS.InputModeShape(:,2);
208 B3 = SYS.InputModeShape(:,3);
209 B4 = SYS.InputModeShape(:,4);
210
211 D1 = SYS.OutputModeShape(1,:);
212 D2 = SYS.OutputModeShape(2,:);
213 D3 = SYS.OutputModeShape(3,:);
214 D4 = SYS.OutputModeShape(4,:);
215
216
217 if BVSetting.DampedMode == 1 % mode decoupling for 1 mode
218 Nu1 = null([B2';B3';B4' ]);
219 Ny1 = null( [D2;D3;D4]);
220
221 elseif BVSetting.DampedMode == 2 % mode decoupling for 2
       mode
222 Nu1 = null([B1';B3';B4']);
223 Ny1 = null([D1;D3;D4]);
224
225 elseif BVSetting.DampedMode == 3 % mode decoupling for 3
       mode
226 Nu1 = null([B1';B2';B4']);
227 Ny1 = null([D1;D2;D4]);
228
229 elseif BVSetting.DampedMode == 4 % mode decoupling for 4
       mode
230 Nu1 = null([B1';B2';B3']);
231 Ny1 = null([D1;D2;D3]);
232 end
233
234 [reZ,imZ] = nyquist(M,wn1);  % norm(reZ.*reZ+imZ.*imZ,2)
235 bnd_min= 0; bnd_max = pi;
236 F = @(phi) -norm( Ny1' * (reZ * cos(phi) + imZ * sin(phi)
       ) * Nu1 ,2);
237 phi_star = fminbnd(F,bnd_min,bnd_max);
238
239
240 Fmat = Ny1'* (reZ * cos(phi_star) + imZ * sin(phi_star))
       * Nu1;
241 [ky_mat,~,ku_mat] = svd(Fmat);
242 ku = ku_mat(:,1);
243 ky = ky_mat(:,1);
244 ku_true=  Nu1 * ku;
```

```
245 ky_true=  Ny1 * ky;
246
247 end
248
249 SYS.ky=ky_true;
250 SYS.ku=ku_true;
251
252 end
253
254 function [SYS] = getInMS(SYS)
255
256
257 Htf_nest=SYS.H;
258 wn = SYS.wn;
259 NumOfPatch = SYS.NumOfPatch;
260 B_result=[];
261
262 for i = 1:length(wn)
263 wn_nest=wn(i);
264 Htf_wn = freqresp(Htf_nest,wn_nest);
265 [Jmin] =  Jcost_nested(Htf_wn);
266 bmi_result = GetBmi(Jmin,NumOfPatch);
267 B_result= [B_result bmi_result];
268 end
269
270 SYS.InputModeShape = B_result;
271
272 end
273
274 function Bmi = GetBmi(Jmin,NumOfPatch)
275 Jresult = Jmin;
276
277 if NumOfPatch == 4
278 Bmi = [cos(Jresult(3))*cos(Jresult(2))*cos(Jresult(1));
       sin(Jresult(3))*cos(Jresult(2))*cos(Jresult(1));sin(
       Jresult(2))*cos(Jresult(1));sin(Jresult(1))];
279
280 elseif NumOfPatch == 3
281 Bmi = [cos(Jresult(2))*cos(Jresult(1));sin(Jresult(2))*
       cos(Jresult(1));sin(Jresult(1))];
282 end
283
284 end
285
286 function [Jmin] =  Jcost_nested(Htf_wn)
```

B

```
287
288 lb=[-pi,-pi,-pi];
289 ub=[pi,pi,pi];
290
291
292 problem.solver = 'ga';
293 problem.fitnessfcn = @JcostNest;
294
295 problem.nvars = 3;
296 problem.lb=lb;
297 problem.ub =ub;
298 problem.options = gaoptimset('PopInitRange',[-pi,-pi,-pi;
        pi,pi,pi]);
299 [Jmin,f,exitflag,output] = ga(problem);
300
301 % Nested function that computes the objective function
302     function J = JcostNest(theta)
303     theta1= theta(1);
304     theta2= theta(2);
305     theta3= theta(3);
306
307     bmi = [cos(theta3)*cos(theta2)*cos(theta1);sin(theta3
            )*cos(theta2)*cos(theta1);sin(theta2)*cos(theta1);
            sin(theta1)];
308
309     Tini = [bmi,null(bmi')];
310     M = Htf_wn * Tini;
311     J = norm(M(:,2:end),1);  % Norm for the null space of
            B.
312     end
313 end
314
315
316 function [SYS] = getOutMS(SYS)
317
318 Htf_nest=SYS.H;
319 NumOfPatch = SYS.NumOfPatch;
320 wn = SYS.wn1;
321 C_result=[];
322
323 for i = 1:length(wn)
324 wn_nest=wn(i);
325 Htf_wn = freqresp(Htf_nest,wn_nest);
326 [Jmin] =  JcostC_nested(Htf_wn);
327 cmi_result = GetCmi(Jmin,NumOfPatch);
```

```
C_result = [C_result; cmi_result];
end

SYS.OutputModeShape = C_result;

end

function Cmi = GetCmi(Jmin,NumOfPatch)
Jresult = Jmin;
if NumOfPatch == 4
Cmi = [cos(Jresult(3))*cos(Jresult(2))*cos(Jresult(1)),
   sin(Jresult(3))*cos(Jresult(2))*cos(Jresult(1)),sin(
   Jresult(2))*cos(Jresult(1)),sin(Jresult(1))];
elseif NumOfPatch == 3
 Cmi = [cos(Jresult(2))*cos(Jresult(1)),sin(Jresult(2))*
    cos(Jresult(1)),sin(Jresult(1))];
end
end

function [Jmin] =  JcostC_nested(Htf_wn)

lb=[-pi,-pi,-pi];
ub=[pi,pi,pi];

problem.solver = 'ga';
problem.fitnessfcn = @JcostNestC;
problem.nvars = 3;
problem.lb=lb;
problem.ub =ub;
problem.options = gaoptimset('PopInitRange',[-pi,-pi,-pi;
    pi,pi,pi]);
[Jmin,f,exitflag,output] = ga(problem);

function J = JcostNestC(theta)

    theta1= theta(1);
    theta2= theta(2);
    theta3= theta(3);
  cmi = [cos(theta3)*cos(theta2)*cos(theta1),sin(theta3)*
     cos(theta2)*cos(theta1),sin(theta2)*cos(theta1),sin(
     theta1)];
    Touti = [cmi;null(cmi).'];

    M = Touti*Htf_wn;
    J = norm(M(2:end),2);
```

```
367 end
```